Acta Pharmaceutica Sinica B 2024;14(8):3493−3512

Chinese Pharmaceutical Association
Institute of Materia Medica, Chinese Academy of Medical Sciences

Acta Pharmaceutica Sinica B

www.elsevier.com/locate/apsb
www.sciencedirect.com

ORIGINAL ARTICLE

Phenylalanine deprivation inhibits multiple myeloma progression by perturbing endoplasmic reticulum homeostasis

Longhao Cheng [a,†], Xiaoxue Wang [b,†], Aijun Liu [c,†], Ying Zhu [c], Hu Cheng [a], Jiangling Yu [a], Lili Gong [a,*], Honglin Liu [a,*], Guolin Shen [d,*], Lihong Liu [a,b,*]

[a]*Institute of Clinical Medical Sciences, China−Japan Friendship Hospital, Capital Medical University, Beijing 100029, China*
[b]*Department of Pharmacy, China−Japan Friendship Hospital, Beijing 100029, China*
[c]*Beijing Chao-Yang Hospital, Capital Medical University, Beijing 100020, China*
[d]*Institute of Chemicals Safety, Chinese Academy of Inspection and Quarantine, Beijing 100020, China*

Received 19 February 2024; received in revised form 8 April 2024; accepted 10 April 2024

KEY WORDS

Multiple myeloma;
Phenylalanine;
Amino acid metabolism;
Nutrient deprivation;
Cancer therapy;
Endoplasmic reticulum stress;
ATF3;
Apoptosis

Abstract Amino acid metabolic remodeling is a hallmark of cancer, driving an increased nutritional demand for amino acids. Amino acids are pivotal for energetic regulation, biosynthetic support, and homeostatic maintenance to stimulate cancer progression. However, the role of phenylalanine in multiple myeloma (MM) remains unknown. Here, we demonstrate that phenylalanine levels in MM patients are decreased in plasma but elevated in bone marrow (BM) cells. After the treatment, phenylalanine levels increase in plasma and decrease in BM. This suggests that changes in phenylalanine have diagnostic value and that phenylalanine in the BM microenvironment is an essential source of nutrients for MM progression. The requirement for phenylalanine by MM cells exhibits a similar pattern. Inhibiting phenylalanine utilization suppresses MM cell growth and provides a synergistic effect with Bortezomib (BTZ) treatment *in vitro* and murine models. Mechanistically, phenylalanine deprivation induces excessive endoplasmic reticulum stress and leads to MM cell apoptosis through the ATF3−CHOP−DR5 pathway. Interference with ATF3 significantly affects phenylalanine deprivation therapy. In conclusion, we have

*Corresponding authors.
E-mail addresses: llh-hong@outlook.com (Lihong Liu), shengl@aqsiqch.ac.cn (Guolin Shen), honglinl2003@163.com (Honglin Liu), gonglili@126.com (Lili Gong).
†These authors made equal contributions to this work.
Peer review under the responsibility of Chinese Pharmaceutical Association and Institute of Materia Medica, Chinese Academy of Medical Sciences.

https://doi.org/10.1016/j.apsb.2024.04.021

identified phenylalanine metabolism as a characteristic feature of MM metabolic remodeling. Phenylalanine is necessary for MM proliferation, and its aberrant demand highlights the importance of low-phenylalanine diets as an adjuvant treatment for MM.

1. Introduction

Multiple myeloma (MM), one of the hematological malignancies, is characterized by the clonal proliferation of plasma cells in the bone marrow (BM). It ranks as the second most prevalent hematological malignancy in the world. As the most populous country, China has the second-highest incidence rate of MM, with an estimated number of 32,000 new MM cases and 27,600 death cases in 2020[1]. Many risk factors are linked to the etiology, such as age, sex, race, and immune system damage[2]. With the growth of the elderly population and significant sex differences, the incidence and mortality of MM are on the rise[3]. Although significant advances in the treatment of MM have prolonged survival, most patients still face drug resistance and relapse. Therefore, MM is still incurable. Knowledge of MM potential mechanisms and new treatment strategies is urgently needed.

Metabolic remodeling is a hallmark of cancer, providing a new perspective for the mechanism research[4]. Theoretically, metabolic remodeling provides the energy and raw materials for cancer cells, which includes nutrients such as glucose, fatty acids, and amino acids[5,6]. For example, tumor cells upregulate glucose or glutamine uptake to meet their metabolic reliance[7–9]. Studies have also shown that hematologic malignancies often rely on certain nutrient to reshape the BM microenvironment, impair immune cell surveillance, promote drug resistance, and ultimately lead to the progression of cancer cells[10–12]. In response to the challenges of cancer treatment, the development of drugs targeting metabolic remodeling has advanced from preclinical to clinical research based on many studies, showing promising therapeutic efficacy[13–15]. Therefore, metabolic remodeling has attractive implications for cancer diagnosis and treatment. On the one hand, abnormal metabolites can serve as potential markers for the malignant proliferation of cancer cells. On the other hand, regulating the metabolic pathways of cancer cells through alterations in nutrient supply or specific metabolic inhibitors is a viable strategy for therapy.

Abnormal amino acid metabolism is one of the characteristics of cancer metabolic remodeling. Amino acids promote protein synthesis and play an important role in energy generation, organic synthesis, and cellular homeostasis[16,17]. Remodeling of amino acid metabolism regulates tumor cell growth from multiple aspects and participates in anti-tumor responses. Asparagine, as an intracellular amino acid regulator, is synthesized by asparagine synthetase. It was reported that asparagine bioavailability strongly influenced metastatic potential[18]. Limiting asparagine through the knockdown of asparagine synthetase, treatment with L-asparaginase, or dietary asparagine restriction reduces the potential for tumor metastasis. In addition, serine, cysteine, and arginine are frequently researched in amino acid metabolic remodeling[19–21]. Therefore, amino acid remodeling plays an essential role in malignant progression and the tumor microenvironment. Focusing on amino acid remodeling facilitates understanding of tumor adaptability and heterogeneity. However, the relationship between amino acid remodeling and MM remains unclear. Targeting MM metabolism requires further in-depth investigations.

Therefore, our investigation aimed to analyze the metabolic alterations of MM. By characterizing metabolic changes within the BM microenvironment and blood circulation, we sought to identify potential metabolic markers for MM treatment. These efforts not only shed light on the metabolic pathogenesis underlying MM but also provide a novel adjuvant therapy for the disease.

2. Materials and methods

2.1. Reagents

Bortezomib (BTZ, HY-10227), carfilzomib (CFZ, HY-10455), dexamethasone (DEX, HY-14648), thalidomide (THA, HY-14658), propranolol (HY-B0573B), tolbutamide (HY-B0401), l-phenylalanine (HY-N0215), L-tyrosine (HY-N0473), Z-VAD-FMK (HY-16658B), acetylcysteine (NAC, HY-B0215), 4-phenylbutyric acid (4-PBA, HY-A0281), BCH (HY-108540), 3-methyladenine (3-MA, HY-19312), Necrostatin-1 (Nec-1, HY-15760), and Ferrostatin-1 (Ferr-1, HY-100579) were purchased from MedChemExpress. $^{13}C_9$-Phenylalanine was purchased from Sigma−Aldrich. Phenylalanine-free, glucose-free, and glutamine-free RPMI-1640 medium was purchased from Beijing Livning Biotechnology Co., Ltd., Beijing, China.

2.2. Clinical samples

Two clinical cohorts were collected for the detection of peripheral blood (PB) plasma and BM. In the analysis cohort, plasma samples were collected from 176 participants, including 33 healthy subjects and 143 newly diagnosed MM patients. BM samples were collected from 114 participants, including 47 patients without malignant tumors and 67 newly diagnosed MM patients. In the validation cohort, plasma samples were collected from 40 healthy subjects and 30 MM patients undergoing treatment. BM samples were collected from 23 patients without malignant tumors and 29 MM patients within treatment. All MM patients were collected from Beijing Chaoyang Hospital between 2019 and 2024 and met the diagnostic criteria of the International Myeloma Working Group guidelines. All MM patients received regular follow-ups. There were no significant metabolic changes in the patients as a result of the various treatment regimens. Blood and BM samples were extracted in the early morning on an empty stomach and stored at −80 °C until metabolite extraction. Clinical information, including gender, age, ISS stage, and cytogenetic aberrations, was collected. This study was approved by the Research Ethics Committee of Beijing Chaoyang Hospital (No. 2019-4-15-4 and the revised version of No. 2021-3-22-3). Each patient provided written informed consent before their participation. Bone marrow aspiration samples from patients were obtained using routine procedures. The research design and methods were carried out in

accordance with the Declaration of Helsinki's Guidelines and all applicable laws regarding the use of human study subjects.

2.3. Untargeted metabolomics analysis

BM samples were centrifuged to separate BM supernatant and BM cells. For all plasma and BM samples, 50 μL of the sample was mixed with 450 μL of regent (methanol:acetonitrile = 1:1, containing internal standards (IS): propranolol 100 ng/mL and tolbutamide 200 ng/mL) to precipitate proteins. After the vortex, the samples were centrifuged, and 100 μL of the sample was then transferred to a new tube for metabolomics analysis. Each sample was mixed for quality control (QC) with the same pretreatment as the study samples. QC samples were evenly inserted in every ten samples to monitor the instrumentation and method stability.

An ultra-performance liquid chromatography and a high-resolution mass spectrometer QE-Orbitrap (UPLC−HRMS) were employed for detection (Thermo Fisher Scientific). Detailed methods for UPLC−HRMS-based untargeted metabolomics were performed as described in Ji et al.[22].

Endogenous metabolites were identified using the mzCloud software. The MetaboAnalyst 5.0 platform was applied to generate principal component analysis (PCA) and orthogonal projections to latent structure discriminant analysis (OPLS-DA) models. Differential metabolite markers were identified based on strict criteria: VIP > 1 and $P < 0.05$. Different metabolic pathways were analyzed using the Pathway Analysis tool in MetaboAnalyst 5.0. Metabolic pathways with an impact value greater than 0.1 were selected as the major differential metabolic pathways.

2.4. Targeted metabolomics analysis

MM cell samples included cell pellets and cell supernatant. Animal samples were derived from mouse serum, femoral bone marrow, and tumor tissues. All samples were treated using the same procedures as those employed in untargeted metabolomics analysis. A regent (methanol:acetonitrile = 1:1, containing IS: propranolol 100 ng/mL and tolbutamide 200 ng/mL) was used as a protein precipitation solution. After vortex and centrifugation, the resulting supernatant was used for quantitative analysis.

Targeted metabolomics was performed using UPLC−HRMS. Chromatographic separation was achieved on a Hypersil Gold C18 Column (Thermo Fisher Scientific, 2.1 mm × 50 mm, 3.0 μm) at a flow rate of 0.3 mL/min, maintained at 30 °C. Mobile phase A was water containing 0.1% formic acid and 2.5 mmol/L ammonium formate, and mobile phase B was acetonitrile. The gradient conditions were as follows: 0−0.5 min, 95%−90% A; 0.5−1.0 min, 90%−70% A; 1.0−2.0 min, 70%−5% A; 2.0−4.0 min, 5%−5% A; 4.0−4.5 min, 5%−95% A; 4.5−6.0 min, 95% A, and the injection volume was 5 μL. The spectrometric settings for positive/negative ion modes were as follows: parallel reaction monitor scan mode, phenylalanine 166.08626/120.08100, tyrosine 182.08117/136.07578, propranolol (IS) 260.16451/116.10709; resolution, 70,000; spray voltage (+), 3.0 kV; capillary temperature, 350 °C; S-lens radio frequency, 50; normalized collision energy, 30. Phenylalanine and tyrosine standards were diluted to a series of gradient concentrations with a 50% methanol aqueous solution. Standard curves were depicted with the peak areas of the phenylalanine and tyrosine standards. Quantification of phenylalanine and tyrosine was calculated based on their respective standard curves.

2.5. Cell culture

Human myeloma cells NCI-H929, RPMI-8226, LAMA-84, and ARD were purchased from the Cell Resource Center, IBMS, CAMS/PUMC. All myeloma cell lines were cultured in RPMI-1640 medium containing 10% fetal bovine serum and penicillin−streptomycin antibiotics. MM cells were cultured in 5% CO_2 at 37 °C. These cells are mycoplasma-free. For phenylalanine starvation, a phenylalanine-free RPMI-1640 medium containing 10% FBS and antibiotics was used.

2.6. Cell viability and cell proliferation assay

Cell viability was assessed by a CCK-8 Kit (Beijing Livning Biotechnology Co., Ltd., Beijing, China). Briefly, a total of 4×10^4 cells/well were plated in 96-well plates, with each well supplemented with 10% FBS in a volume of 100 μL medium. After 48 h of amino acid starvation, the CCK-8 reagent (10 μL/well) was added, and the reaction solution was incubated at 37 °C for 2 h. The absorption was then measured at 450 nm using a microplate reader. To assess cell viability recovery, MM cells were incubated with phenylalanine-free RPMI-1640 medium along with various concentrations of phenylalanine for 48 h.

Cell proliferation was determined with a BeyoClick EdU Proliferation Assay Kit (Beyotime, Shanghai, China) following the manufacturer's instructions. MM cells were labeled with EdU and Alexa Fluor 488 Azide. Cells were visualized using an Olympus fluorescence microscope.

2.7. Flow cytometry analysis of cell cycle and apoptosis

Commercial detection kits (Keygen Biotech, Nanjing, China) were applied to analyze cell cycles. Briefly, after 48 h of phenylalanine deprivation, MM cells (1×10^6 cells) were fixed with 70% ethanol overnight and then incubated with an RNase/PI staining solution for 30 to 60 min. Flow cytometry was used to determine the DNA content at different phases of the cell cycle. Red fluorescence was recorded at the excitation wavelength of 488 nm.

Commercial detection kits (BD Bioscience, USA) were applied to analyze cell apoptosis. Briefly, after 48 h of phenylalanine deprivation, MM cells (5×10^5 cells/mL) were harvested and resuspended in a binding buffer. Then, Annexin V-FITC and 7-AAD were added to stain the cells. The stained cells were sorted and quantified by the flow cytometer to detect apoptotic cells.

2.8. Reactive oxygen species (ROS) detection

The levels of ROS in MM cells were detected by a ROS Assay Kit (Beyotime, Shanghai, China) according to the manufacturer's instructions. Briefly, MM cells (1×10^6 cells/mL) were harvested and incubated with 10 μmol/L 2′,7′-dichlorofluorescin diacetate (DCFH-DA) to detect the intracellular ROS level. After incubation at 37 °C for 30 min, the cell pellets were collected and washed twice with PBS to remove the residual DCFH-DA probe. Samples were measured for fluorescence at 488 nm excitation and 525 nm emission using a microplate reader. Protein concentration was analyzed by the BCA assay kit to obtain a quantitative result.

2.9. Glutathione (GSH) level detection

GSH levels were detected by a GSH Assay Kit (Beyotime, Shanghai, China) according to the manufacturer's instructions. Briefly, MM cells (5×10^6 cells/group) were incubated with a fluorescent reagent, 5,5′-dithiobis-(2-nitrobenzoic acid) at room temperature, followed by the addition of 0.5 mg/mL NADPH. Finally, the absorbance was measured at 412 nm, and the GSH content was determined based on a calibration curve using GSH standards.

2.10. Transfection of cell

MM cells (4×10^5 cells/mL) were inoculated in 6-well plates one day ahead. Then, siRNAs (30 pmol) and Lipofectamine RNAiMAX (Thermo Fisher Scientific) were diluted with Opti-MEM Medium. Diluted siRNAs and diluted Lipofectamine RNAiMAX were added to the cells. RNA and protein expression were validated 72 h after transfection. siRNAs against DNA Damage Inducible Transcript 3 (DDIT3), Activating Transcription Factor 3 (ATF3), and TNF receptor superfamily member 10b (TNFRSF10B), as well as negative control siRNAs, were constructed by Syngentech Co., Ltd., Beijing, China. The sequences of siRNAs are presented in the Supporting Information Table S1.

2.11. Plasmid construct and dual luciferase assay

The pDR5-WT plasmid, pDR5-mutant plasmid, and ATF3 overexpression plasmid were constructed. The mutant sequence of ATF3-binding sites in the pDR5-mutant plasmid was 5′-GGTGACGACACC-3′. Cells were co-transfected with the pGL4.10-MCS-luc2 vector, which was connected with Firefly luciferase and Renilla luciferase (pGL4.74), along with the AT3 overexpression sequence and death receptor 5 (DR5) promoter region. Lipofectamine 3000 (Thermo Fisher Scientific) was used to transfect the plasmids according to the manufacturer's instructions. After 48 h of incubation, luciferase activity was detected by the Dual-Luciferase Reporter Assay Kit (MeilunBio, Dalian, China) and normalized based on Renilla luciferase activity.

2.12. RNA isolation and RT-qPCR

Total RNA was extracted using RNAiso Plus Reagent (TaKaRa Biotech, Dalian, China) according to standard procedures. Purified RNA was reverse transcribed into cDNA through the reaction mixture using the cDNA Synthesis Kit (Vazyme Biotech, Nanjing, China) according to the manufacturer's protocol. Then, a real-time PCR reaction mixture was prepared, which included cDNA, gene primers, and SYBR Green, using a TAQ Pro Universal SYBR qPCR Kit (Vazyme Biotech, Nanjing, China). The primer sequences designed for each gene are shown in the Supporting Information Table S2.

2.13. Western blotting

Western blotting was performed as previously described[23]. Primary antibodies used were as follows: anti-β-actin (Cell Signaling Technology, 4967, 1:3000), anti-p-PERK (Proteintech, 29546-1-AP, 1:1000), anti-PERK (Proteintech, 24390-1-AP, 1:1000), anti-p-eIF2α (Proteintech, 28740-1-AP, 1:1000), anti-eIF2α (Proteintech, 11170-1-AP, 1:1000), anti-ATF4 (Proteintech, 10835-1-AP, 1:1000), anti-Caspase-8 (Proteintech, 13423-1-AP, 1:1000), anti-PARP (Proteintech, 13371-1-AP, 1:1000), anti-VAPB (Proteintech, 14477-1-AP, 1:1000), anti-CHOP (Cell Signaling Technology, 2895, 1:1000), anti-cleaved caspase-3 (Cell Signaling Technology, 9661, 1:1000), anti-ATF3 (Santa Cruz, sc-81189, 1:200), and anti-DR5 (Proteintech, 15497-1-AP, 1:1000). The band strength was analyzed by a gel documentation system. Row values were quantified by ImageJ to calculate the relative protein abundance.

2.14. In vivo experiments

Five-week-old NOG mice (male, 18−20 g) were purchased from Vital River Laboratory Animal Technology (Beijing, China) and were raised under specific pathogen-free housing conditions. All procedures involving animal studies were ethically approved by the China−Japan Friendship Hospital Institutional Animal Ethics Committee. After one week of acclimatization, mice were randomly divided into different groups ($n = 5$ mice per group). To construct the xenograft model, each mouse was injected subcutaneously with NCI-H929 cells (5×10^6 cells/0.1 mL injection in PBS). Weight growth was monitored weekly, and tumor volumes were calculated by measuring length $\times$ width^2/2. After three weeks, mice were euthanized when the maximal tumor diameter did not exceed 2.5 cm. Serum was collected immediately and used for metabolomics studies. Solid tumors were separated and fixed for hematoxylin−eosin staining and immunohistochemical staining. Residual tumor tissue was further analyzed by Western blotting.

To construct the orthotopic transplantation model, each mouse was injected intravenously with luciferase-labeling RPMI-8226 cells (5×10^6 cells/0.1 mL injection in PBS). Weight growth was monitored weekly, and tumor burden was assessed using *in vivo* imaging systems and micro-computed tomography (micro-CT) scans of femurs after six weeks. Serum was separated, and bone turnover markers (serum PINP, serum ICTP, and serum lambda free light chains (λFLC)) were quantified by ELISA (Enzyme-linked Biotech, Shanghai, China). Serum calcium and ALP levels were measured with commercial kits (Nanjing Jiancheng Bioengineering Institute, Nanjing, China). The femurs were examined by histopathology. The control diet (A02082003B) and phenylalanine-free diet were purchased from Xietong Pharmaceutical Bioengineering Co., Ltd., Jiangsu, China. The nutrients in the control diet were prepared according to the prescribed formula. The phenylalanine-free diet contained all the same nutrients as the control diet, except for phenylalanine and corn starch. The lack of nutrition was offset by increased corn starch levels due to phenylalanine deficiency. After one week of MM modelling, treatments were administered until the endpoints of the experiments. Mice were injected intraperitoneally with BTZ (0.5 mg/kg) twice a week during the administration. The mice in the control groups were injected with saline simultaneously.

2.15. In vivo imaging and micro-CT scanning

Bioluminescence imaging (BLI) was performed using an IVIS Lumina Series III Imaging System. Briefly, mice were intraperitoneally injected with D-luciferin potassium salt (15 mg/mL) and then anesthetized with isoflurane. After 10 min post-injection, luminescence signals were obtained using an exposure time set to "Auto" and a binning value of 8. To quantify signal intensity, the regions of interest were selected and calculated.

The distal femur and lumbar vertebrae of the mice were scanned with a high-resolution micro-CT system (Siemens Inveon

MM GANTRY, Germany). Bone parameters were then calculated using Inveon Research Workplace software, which included bone density parameters and bone structure parameters.

2.16. RNA-Seq data processing

Using the polyA enrichment method, RNA-Seq libraries were constructed. These libraries were sequenced using the Illumina NovaSeq 6000 platform. The reference genome and gene annotation files were downloaded from the genome website. Filtered reads were mapped to the reference genome using HISAT2 v2.0.5. We used HTSeq statistics to compare the Read Count values for each gene with the original gene expression, and subsequently normalized the expression using FPKM. Then, discrepancies in gene expression were analyzed by DESeq (version 1.39.0) with the following criteria: multiple expression differences $|\log2FoldChange| > 1$ and a significant P-value < 0.05. A two-way cluster analysis of all genes expressed differentially in the samples was performed using R software (version 4.3.1). Next, Gene Set Enrichment Analysis (GSEA) of all detected genes was performed by GSEA software (version 3.0), which analyzed the differences in biological functions between two groups based on gene sets.

2.17. Isotope tracing

Isotope tracing was performed according to the established protocol. Briefly, NCI-H929 cells cultured in phenylalanine-free medium (supplemented with 10% FBS) were added 10 mg/L of $^{13}C_9$-phenylalanine. Cells were collected after 0, 6, 12, and 24 h of cultivation. The samples collected at 0 h were used for calibration. Cell pellets were washed with PBS and used for metabolic flow detection. Procedures for detection methods and data analysis were described[24,25]. Internal calibration of the samples was performed using l-leucine-d10 as an internal standard, and normalization was carried out based on protein content.

2.18. Immunofluorescence staining

NCI-H929 cells were attached to polylysine-coated cell slides overnight at 37 °C and 5% CO_2. Subsequently, the cells were treated with phenylalanine deprivation for 48 h. Cells were washed with PBS, fixed in 4% paraformaldehyde for 20 min, and permeabilized with 0.2% Triton X-100 in PBS for 10 min. After being blocked with 5% BSA for 30 min, cells were incubated with DR5 antibody (Cell Signaling Technology, 8074, 1:500) and Caspase-8 antibody (Proteintech, 13423-1-AP, 1:100) at 4 °C overnight. Then, the DR5 antibody was combined with the rabbit HRP-labeled secondary antibody and incubated with the third antibody, Cy3-conjugated Affinipure Donkey anti-goat IgG (H+L), for 1 h. The caspase-8 antibody was incubated with Alexa Fluor 488 for 1 h. Cells were incubated with Hoechst 33342 for 10 min in the dark. Finally, the cells were analyzed using a Zeiss LSM800 confocal laser microscope.

2.19. Transmission electron microscopy (TEM)

TEM analysis was used to observe cell apoptosis and endoplasmic reticulum morphology of MM cells. Briefly, NCI-H929 cells were treated with phenylalanine deprivation for 48 h. Cells were then collected and fixed in 4% glutaraldehyde. Next, cells were processed with fixation, dehydration, embedding, and curing. Ultrathin sections were stained with 3% uranium acetate-lead citrate and visualized using a JEOL JEM-1400 Plus (100 kV) TEM instrument.

2.20. Drug affinity−responsive target stabilization assay (DARTS)-proteomics

Approximately 5×10^6 NCI-H929 cells were lysed on ice for 20 min using M-PER (Thermo Fisher Scientific). The lysates (1 mg/mL) were incubated with PBS or 100 μmol/L phenylalanine in 1× TNC buffer. This incubation was performed overnight at 4 °C to facilitate the formation of ligand−protein complexes. The lysates were then digested with *Streptomyces griseus* protease at a ratio of 1:1000 for 30 min. The reaction was terminated by adding the loading buffer and then boiling for 10 min. The resulting samples were then separated by SDS-PAGE and stained with Coomassie Blue. Nanoflow LC−MS/MS analysis was used to identify differences in protein abundance between gel bands with and without the addition of phenylalanine. MS spectra were searched against the Uniprot Homo sapiens Swiss-Prot proteome database. The GO and KEGG databases were used to analyze the protein family and pathways.

2.21. Cellular thermal shift assay (CETSA)

Approximately 5×10^6 NCI-H929 cells were lysed on ice for 20 min using M-PER (Thermo Fisher Scientific). After centrifugation, the supernatant was divided equally into aliquots. Samples were then incubated with 100 μmol/L phenylalanine or PBS for 1 h at room temperature and then heated at different temperatures for 3 min. After centrifugation, the supernatant was mixed with loading buffer and boiled for 10 min. All samples were analyzed by Western blotting.

2.22. Molecular docking

AutoDock Vina was used for molecular docking. The VAPB protein structure was downloaded from the UniProt database, and the structure of the small molecule l-phenylalanine was downloaded from the PubChem database. Pymol software was used for the removal of organics, and AutodockTools was used for hydrogenation, checking charges and docking. Docking scores have been calculated. Binding energy analysis and visualization were performed using PyMOL and Discovery Studio software.

2.23. Statistical analysis

For all analyses of cell lines, the experiments were biologically repeated three times. All data were presented as means ± standard error of mean (SEM). Unpaired two-sided t-tests were used to compare two experimental groups, while one-way ANOVA tests were utilized for comparing three or more experimental groups. P value below 0.05 was considered statistically significant. The analysis was performed using GraphPad Prism 8.0.

3. Results

3.1. Metabolomics workflows for the study cohorts

The workflows are shown in Fig. 1A. Briefly, clinical samples (analysis cohort) were collected from both the control population and MM patients. BM samples were separated into BM

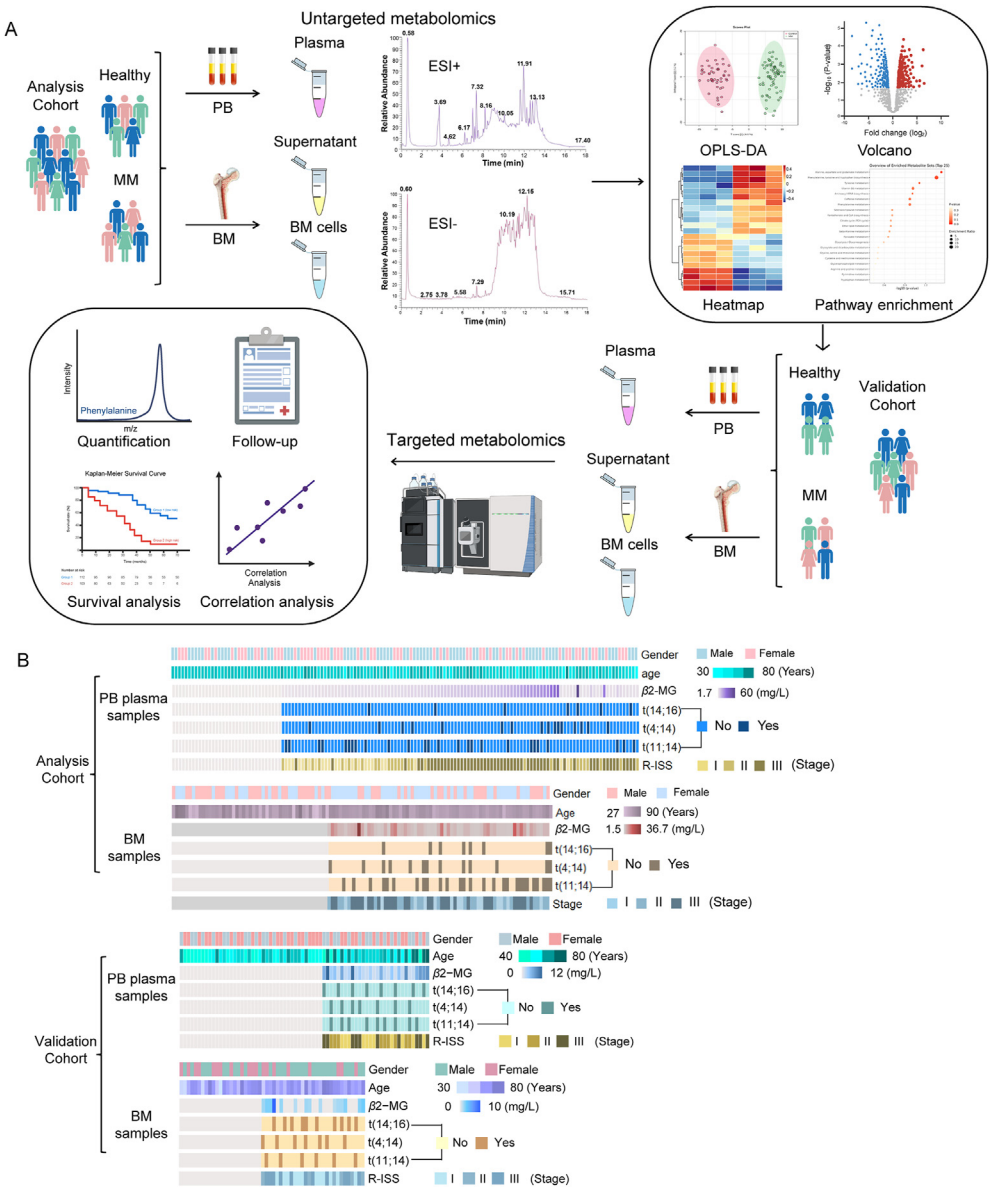

Figure 1 Workflows and demographics of clinical metabolomics. (A) Metabolomics was conducted in the analysis cohort (plasma samples: $n = 33$ in the healthy group, $n = 143$ in the MM group; BM samples: $n = 47$ in the non-cancer group, $n = 67$ in the MM group) and validation cohort (plasma samples: $n = 40$ in the healthy group, $n = 30$ in the MM group; BM samples: $n = 23$ in the non-cancer group, $n = 29$ in the MM group). The BM samples were centrifuged and separated into BM supernatant and BM cells. All samples were detected in both ESI (+/−) ion modes. TIC chromatograms from UPLC/MS detection exhibited typical peak features. Multivariate statistical analysis included OPLS-DA, volcano plots, heatmaps, and pathway enrichment analysis. Targeted metabolomics includes metabolite quantification, patient follow-up, prognostic analysis, and correlation analysis. (Image created with BioRender.com with permission). (B) Baseline demographics and patient characteristics in the analysis cohort and validation cohort included the population's gender, age, serum β2-microglobulin, FISH and R-ISS staging score.

supernatant and BM cells, both of which were analyzed for metabolic changes using untargeted metabolomics. Following multivariate statistical and pathway enrichment analysis, we identified potential biomarkers and altered metabolic pathways associated with MM. The potential biomarker was further validated in an independent database (validation cohort). The demographics of the study cohorts are shown in Fig. 1B. No gender or age differences were found between the control population and MM patients, in order to exclude metabolic differences caused by gender and age. All MM patients met the International Myeloma Working Group criteria for MM.

To uncover the relationship between metabolic changes and MM, we compared three different types of clinical samples: PB plasma samples, BM supernatant, and BM cell samples. Typical total ion chromatograms (TIC) in both ESI^+ and ESI^- modes were displayed (Fig. 1A). To correct systematic errors and control inter-batch variability, stability, and reproducibility, QC samples were employed. We visualized the initial features of all samples using PCA as an unsupervised algorithmic model (Supporting Information Fig. S1A). We further established an OPLS-DA, a supervised multivariate statistical model, for differential metabolite screening. Our results showed that the OPLS-DA models

significantly separated the groups without overfitting (Fig. S1B). The OPLS-DA parameters R2Y and Q2 were used to evaluate the explanatory and predictive capabilities. Our results yielded values ranging from 0 to 1, indicating the effectiveness of the models (Fig. S1C). These results indicate that the diversity of clinical samples is adequate for metabolomics analysis. Through the identification of metabolites, we categorized them into several groups, covering amino acids, organic acids, nucleotides, nucleosides, organic amines, acylcarnitines, vitamins, carbohydrates, and lipids. Notably, the proportion of lipids, organic acids, and amino acids dominated the composition (Fig. S1D). This suggests that abnormal amino acid metabolism plays an important role in MM.

3.2. *Phenylalanine metabolism is disturbed and phenylalanine is a potential biomarker for MM*

To screen candidate biomarkers, VIP values were derived for each metabolite based on the OPLS-DA models, while FC and *P* values were determined by the fold change and significance of intergroup variation, respectively. The detailed information on the main metabolites is provided in Supporting Information Data S1. Specifically, the values of phenylalanine met the following criteria: VIP > 1, $P < 0.05$, and FC > 1.2 (Fig. 2A). Furthermore, pathway enrichment analysis revealed that the phenylalanine-associated pathway is a significant perturbation in all groups (Fig. 2B). Semi-quantitative analysis further suggested that phenylalanine levels decreased significantly in the PB plasma of MM, whereas they increased significantly in both BM supernatant and BM cells (Fig. 2C). This suggests that phenylalanine is transferred from PB to BM during MM progression, where it is utilized by proliferating malignant MM cells. In addition, the levels of tyrosine were comparable to those of phenylalanine, reflecting the effects of phenylalanine metabolic perturbations on downstream metabolites (Supporting Information Fig. S2A). A receiver operating characteristic (ROC) curve of phenylalanine was conducted and revealed that phenylalanine levels in PB plasma can effectively distinguish MM patients from the healthy population, exhibiting good specificity and sensitivity. The area under the curve (AUC) for BM supernatant samples (AUC $= 0.753$) was lower than that for PB plasma samples (AUC $= 0.98$), indicating that phenylalanine can serve as a potential biomarker for MM (Fig. S2B). In addition, samples from MM patients undergoing treatment were collected to serve as a validation cohort for examining the alterations in phenylalanine levels. Quantitative analysis revealed an increase in plasma phenylalanine levels after drug treatment, accompanied by a decrease in BM phenylalanine levels (Fig. S2C). Despite the heterogeneity observed in plasma results, the elevated phenylalanine in plasma underscore the necessity of limiting phenylalanine concentrations. This is attributed to the dual consequences of excessive phenylalanine: on one hand, it poses neurotoxic risks, and on the other, it potentially accelerates the aberrant metabolism of myeloma cells, thereby facilitating the recurrence or malignant progression of MM. Survival analyses showed that patients with low plasma phenylalanine experienced shorter survival times and poorer treatment outcomes during follow-up, while patients with high phenylalanine levels responded better to treatment and had longer survival times (Fig. 2D). This also predicts that plasma phenylalanine levels correlate with the severity of MM and that phenylalanine can serve as a potential diagnostic marker for MM.

To investigate the cause of the phenylalanine metabolic perturbation, stable isotope-labeled phenylalanine was added exogenously under phenylalanine-free conditions (Fig. 2E). Using metabolic flow analysis, the biological functions of phenylalanine and tyrosine were examined. Metabolic tracing with $^{13}C_9$-phenylalanine suggested that phenylalanine (M+8, M+9) was primarily metabolized into tyrosine (M+1, M+2) and tryptophan (M+1, M+2), which were then further metabolized into the tricarboxylic acid (TCA) cycle. The TCA cycle provides energy for biological activities and acts as the hub for the synthesis and conversion of glucose, lipids, and proteins. The levels of LysoPC (M+1), LysoPE (M+1), isoleucine (M+1, M+2), leucine (M+1, M+2), inosine (M+1), hypoxanthine (M+1), xanthine (M+1), and uracil (M+1, M+2) increased over time, suggesting that phenylalanine participates in the synthesis of lipids, amino acids, and nucleotides (Supporting Information Fig. S3A and S3B). However, due to the limitations of the detection conditions, some metabolites did not show isotopically labeled signals, although they are essential substances in the phenylalanine metabolic pathway. Above all, we propose that after phenylalanine is taken up, its principal metabolites in MM cells satisfied the energy requirements for cell proliferation and metabolism. This raises the possibility that exogenous deprivation of phenylalanine could inhibit MM progression.

3.3. *Phenylalanine deprivation inhibits MM in vitro*

To explore whether MM cells and BM cells share similar metabolic characteristics, we quantitatively detected phenylalanine targeting in four MM cell lines (NCI-H929, RPMI-8226, LAMA-84, and ARD). The results revealed that extracellular phenylalanine content was reduced, and intracellular phenylalanine content was elevated in all MM cell lines compared to normal B lymphocytes (Supporting Information Fig. S4A). Furthermore, the expression of L-type amino acid transporters (LATs) involved in phenylalanine transport was upregulated, showing that MM cells showed an abnormal preference for phenylalanine transport (Fig. S4B). BCH, a pan-LATs inhibitor, was used to further confirm whether inhibiting phenylalanine transport could affect MM growth. We discovered that BCH effectively suppressed the survival of MM cells. Treatment with BCH impaired cellular uptake of phenylalanine and increased extracellular phenylalanine levels (Fig. S4C and S4D). Based on these findings, we propose the hypothesis that phenylalanine is an important nutrient that supports MM growth. Phenylalanine deprivation could inhibit MM cells *in vitro*.

To investigate the impact of phenylalanine deprivation on MM *in vitro*, we designed a phenylalanine-free medium to create an external environment conducive to phenylalanine deprivation. As expected, when MM cells were subjected to a phenylalanine-free culture, their cell viability and proliferation rate were substantially inhibited (Fig. 3A). Surprisingly, these effects could be restored with phenylalanine supplementation. The recovery of cell viability exhibited a concentration-dependent response to phenylalanine supplementation (Fig. 3B). Furthermore, phenylalanine deprivation demonstrated a negligible effect on normal BM cells while exhibiting selectivity on MM cells (Fig. S4E). It was also suggested that phenylalanine, as a nutrient, is of comparable importance to glucose and glutamine for cellular metabolism, because glucose or glutamine deprivation can also inhibit cell survival (Fig. S4F and S4G). Based on these findings, we concluded that phenylalanine is an essential nutrient for MM cell proliferation, and its deficiency can inhibit cell growth.

Limiting phenylalanine intake *in vitro* slowed tumor growth, as evidenced by the reduced rate of cell proliferation. We observed that when MM cells were cultured in a phenylalanine-free

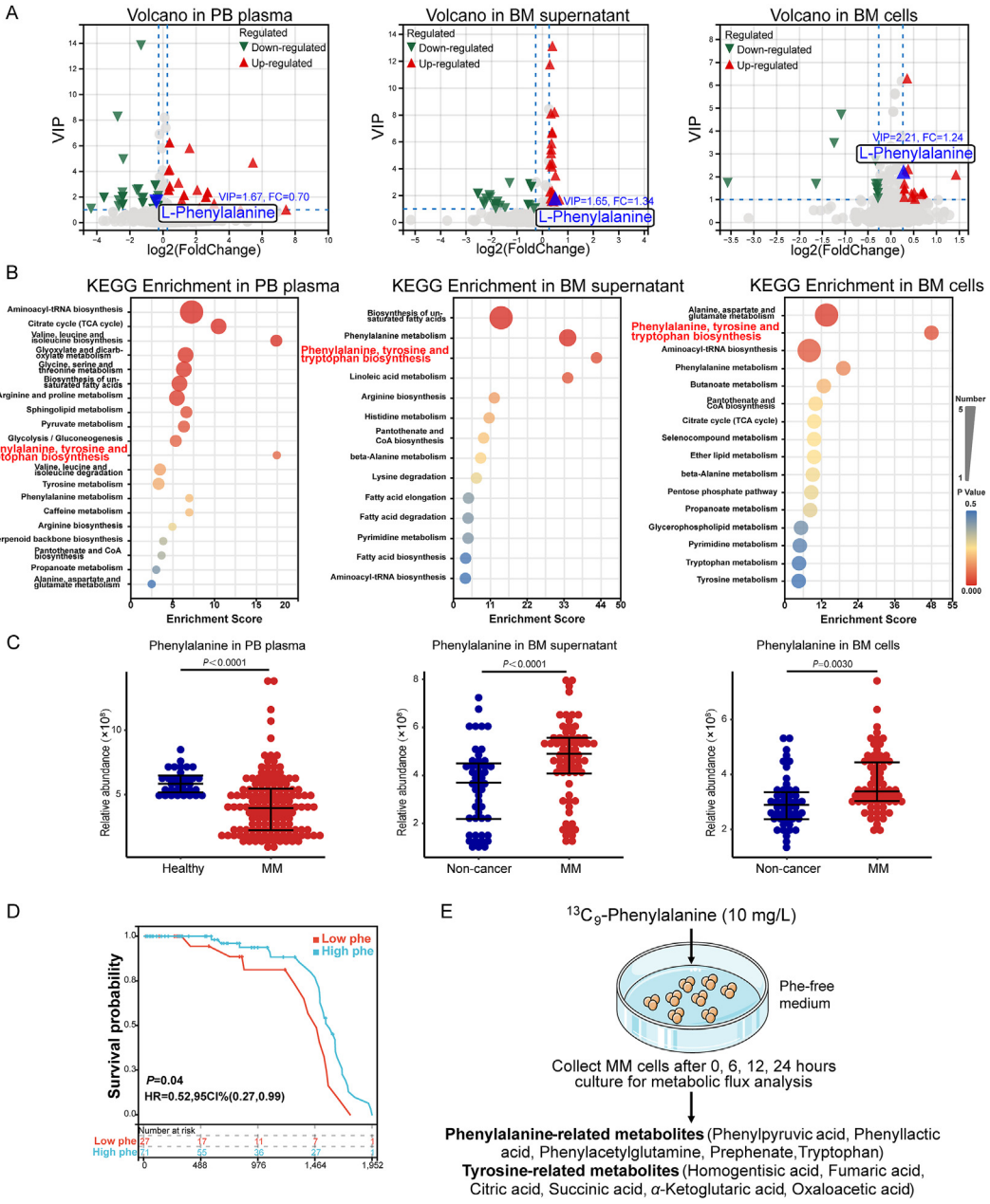

Figure 2 Metabolomics reveals that MM progression is associated with abnormal phenylalanine metabolism. (A) Volcano plots of the differential metabolites with VIP > 1 and FC > 1.2 in PB plasma (n = 33 in the healthy group, n = 143 in the MM group) and BM (divided into supernatant and cells: n = 47 in the non-tumor group, n = 67 in the MM group) groups. Green arrows represent downregulated metabolites, and red arrows represent upregulated metabolites. l-Phenylalanine VIP and FC values are shown and meet the screening criteria. (B) KEGG pathway enrichment analysis shows the top 20 altered metabolic pathways in PB plasma and BM samples. Among them, the pathways associated with phenylalanine metabolism are significantly affected. The color of the plots represents the significance of the pathway, and the volume represents the degree of metabolite enrichment. (C) Semi-quantitative results of phenylalanine in PB plasma and BM samples. (D) Survival analysis showed the relationship between phenylalanine levels and overall survival. (E) Schematic of the phenylalanine metabolic flux experiments. Data are shown as mean ± SEM; an unpaired two-sided t-test was applied.

environment, the cell density was significantly lower (Fig. 3C). To further investigate why phenylalanine deprivation inhibits cell proliferation, we used flow cytometry to monitor the cell cycle. The results revealed that phenylalanine deprivation can cause cell cycle arrest at G0/G1, decrease the proportion of cells in the S phase, and slightly reduce the proportion of cells in the G2 phase (Fig. 3D). This indicates that phenylalanine deprivation limits the rapid proliferation of MM cells, as evidenced by the arrest of the cell cycle.

When tumor cells experience a shortage of amino acids, it is possible to maintain cellular homeostasis[26]. However, severe deprivation of amino acids can disrupt homeostasis, inhibit cell growth, or even cause programmed cell death. Cell death induced by amino acid starvation can be divided into

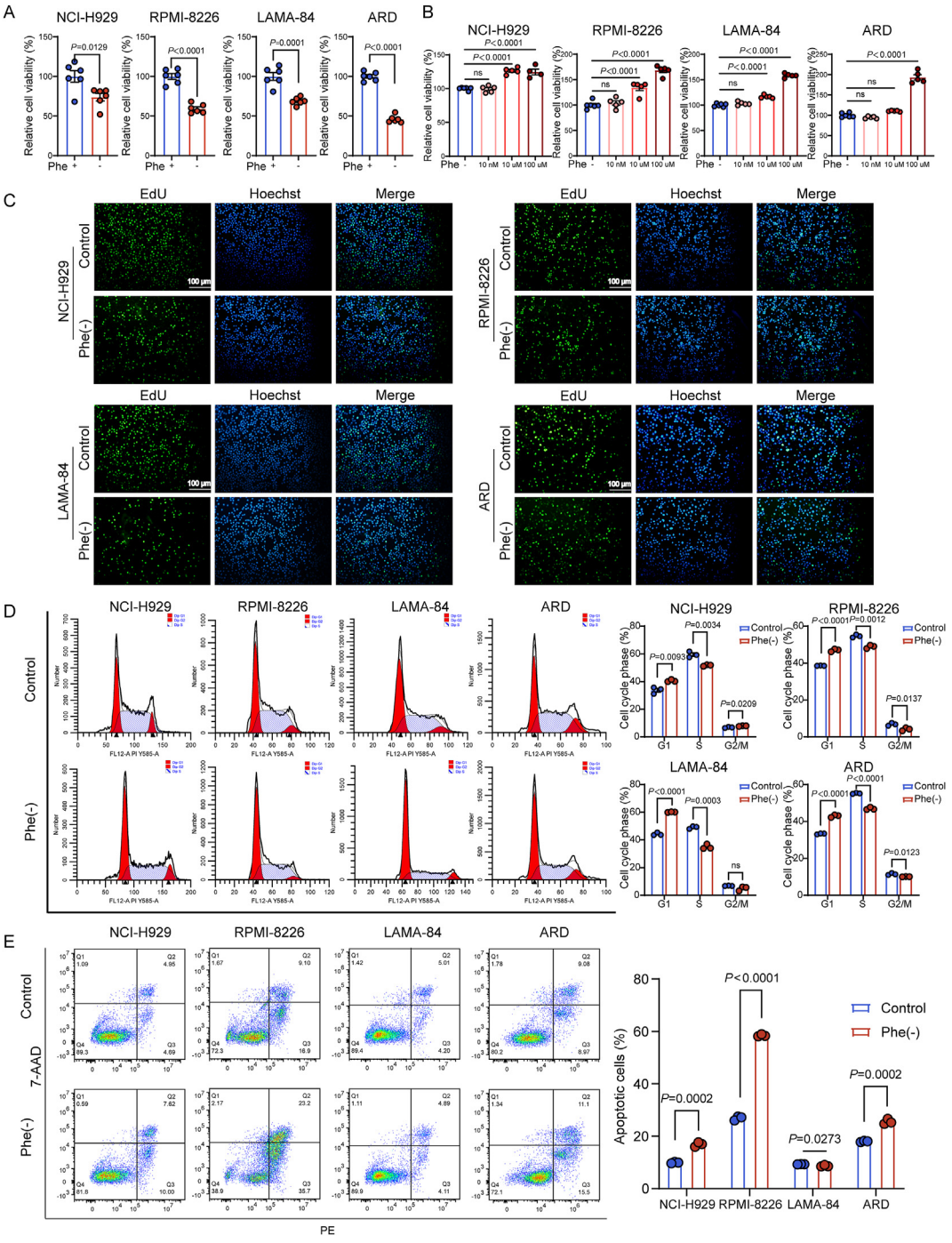

Figure 3 Phenylalanine deprivation inhibits MM *in vitro*. (A) Cell viability of MM cell lines after 48 h of phenylalanine deprivation. (B) Cell vitality of MM cell lines after supplementing the phenylalanine-free medium with varying concentrations of phenylalanine (0, 10 nmol/L, 10 μmol/L, 100 μmol/L) for 48 h of culture. (C) The EdU proliferation assay shows the influence on the proliferation rate of MM cell lines after 48 h of phenylalanine deprivation. Scale bar: 100 μm. (D) Flow cytometry analyzes the effects on the cell cycle of MM cell lines after 48 h of phenylalanine deprivation. (E) Annexin V-PE/7-AAD apoptosis detection in flow cytometry was applied to MM cell lines after 48 h of phenylalanine deprivation. Data are shown as mean ± SEM; $n \geq 3$. Significance was analyzed with an unpaired two-sided *t*-test in (A, D, E) and a one-way ANOVA test in (B). M, mol/L.

caspase-dependent apoptosis and autophagic cell death[13]. However, our findings suggest that phenylalanine deprivation-induced cell death is not related to autophagy (Supporting Information Fig. S6A). To investigate whether phenylalanine deprivation induces apoptosis in MM cells, we conducted Annexin V-PE/7-AAD apoptosis detection. The total number of cells undergoing early and late apoptosis was used for calculating the number of apoptotic cells. Our results indicate that phenylalanine deprivation obviously induces apoptosis in RPMI-8226 cells, followed by NCI-H929 and ARD cells, while

it barely affects LAMA-84 cells (Fig. 3E). In conclusion, phenylalanine is essential for the proliferation of MM cells. Insufficient phenylalanine can inhibit cell proliferation, cause cell cycle arrest, and induce apoptosis.

3.4. *Phenylalanine deprivation inhibits MM in vivo*

We selected NCI-H929 and RPMI-8226, two MM cell lines sensitive to phenylalanine deprivation, for *in vivo* experimental research. RPMI-8226 cells are commonly used in constructing orthotopic xenograft models of MM. The incorporation of the luciferase gene enables bioluminescence imaging for tumor burden evaluation[27]. On the other hand, NCI-H929 cells are commonly used in heterotopic xenograft models of MM. The selection of this cell line not only broadens the tumor spectrum in animal models but also offers advantages due to its rapid growth rate, high tumorigenicity, and ease of handling.

To determine whether exogenous deprivation of phenylalanine could inhibit MM *in vivo*, we pre-fed NOG mice with both normal and phenylalanine-free diets for one week before injecting MM cells to establish the models (Fig. 4A and F). Tumor volumes were measured after one week of model construction to assess tumor burden and the therapeutic effect of phenylalanine deprivation by observing weight, tumor weight, and tumor morphology (Fig. 4B and C). Quantitative detection of serum and tumor tissue phenylalanine levels indicated a significant decrease following phenylalanine restriction, proving the efficacy of a phenylalanine-free diet (Fig. 4D). Furthermore, the levels of tyrosine, the direct metabolic product of phenylalanine, also decreased (Supporting Information Fig. S5A). This suggests that restricting phenylalanine *in vivo* is crucial for MM inhibition. Our data also showed that tyrosine restriction could not effectively inhibit the formation of MM tumors (Fig. S5D and S5K), thus emphasizing the importance of phenylalanine deprivation as a nutritional therapy. Immunohistochemistry on tumor tissues revealed significant increases in necrotic areas of tumors after phenylalanine deprivation. Tumor cells exhibited nuclear shrinkage and rupture with intense staining, indicating an increase in apoptotic cells (Fig. 4E). These results suggest that phenylalanine deprivation exerts an inhibitory effect on the NCI-H929 mouse model.

In the orthotopic transplantation model, luciferase-transfected RPMI-8226 cells were intravenously injected into NOG mice. Similarly, phenylalanine-deprivation diets influenced mouse body weight, which remained stable and within acceptable limits (Fig. 4G). Then, the concentrations of phenylalanine and tyrosine in serum and tibial BM were examined (Fig. 4H and Fig. S5B). These concentrations were significantly reduced, implying abnormal absorption and metabolism of phenylalanine. To assess the extent of MM cell proliferation and BM damage, we measured levels of serum calcium, bone resorption marker ICTP, bone formation markers ALP and PINP, and λFLC secreted by RPMI-8226 cells (Fig. 4J). Serum calcium is a crucial indicator of bone metabolism and reconstruction. ICTP, originating from damaged bone matrix, reflects the degree of bone dissolution[28]. Bone ALP indicates osteoblast activity, while PINP represents the ability of osteoblasts to synthesize collagen. The λFLC represents the proliferation of MM cells[29]. We found that phenylalanine deprivation significantly reduced serum calcium levels, inhibited bone absorption and metabolism, promoted bone reconstruction, and suppressed the rapid proliferation of MM cells, thus reducing bone damage.

The bone damage was also validated by BLI. After phenylalanine deprivation, the area of MM cells located in the femurs and vertebrae decreased, along with the bioluminescence intensity (Fig. 4I). Furthermore, micro-CT scans and hematoxylin and eosin (HE) staining of the distal femur and lumbar vertebrae revealed that the phenylalanine-deprivation group exhibited fewer losses in the trabecular structures of the femurs and lessened vertebral erosion (Fig. 4L and Fig. S5C). Three-dimensional bone structure parameters indicated that phenylalanine deprivation increased bone volume fraction (BV/TV), trabecular number, and trabecular thickness while decreasing bone surface area to volume ratio (BS/BV) and trabecular spacing (Fig. 4K). Therefore, *in vivo* phenylalanine deprivation can inhibit the progression of MM.

3.5. *VAPB as a direct sensor of phenylalanine in MM*

We then used the DARTS-proteomics method to investigate the intracellular binding sites of phenylalanine after administering it exogenously (Fig. 5A). This research aimed to identify potential target proteins to elucidate the direct molecular sensor of phenylalanine. Our findings indicated that protein expression levels were altered after the uptake of phenylalanine, leading to a significant enrichment of these proteins within the endoplasmic reticulum (ER) membrane structures. These proteins are involved in ER formation and protein heterodimerization activities. Specifically, changes of VAPB protein were closely associated with the mentioned characteristics (Fig. 5B, Fig. S6A and S6B). The presence of a phenylalanine motif within the VAPB protein structure provides theoretical evidence for the interaction between phenylalanine and VAPB. Experimental studies also revealed widespread expression of VAPB protein in MM cells (Fig. 5C and D). Through molecular docking simulations, we assessed the binding capacity of phenylalanine to VAPB (Fig. 5E). Furthermore, the CETSA method was utilized to verify that phenylalanine improved the stability of the VAPB protein (Fig. 5F). Interference with VAPB expression impacted the restorative effects of phenylalanine on MM cells (Fig. 5G and H), affecting cellular processes such as proliferation, cell cycle, and apoptosis (Fig. 5I−K). Consequently, our research supports the findings that phenylalanine directly interacts with the VAPB protein.

3.6. *Mechanism of phenylalanine deprivation in inhibiting MM progression*

Our research has provided compelling evidence that phenylalanine deprivation can inhibit MM. To elucidate the mechanism by which phenylalanine deprivation inhibits MM progression, we used RNA-sequencing on MM cells and assessed differential gene expression after phenylalanine deprivation. The differential gene selection criteria were $|\log2FC| > 1$ and $P < 0.05$. In NCI-H929 cells, we identified 2487 differential genes, including 1573 upregulated genes and 914 downregulated genes. In RPMI-8226 cells, we identified 114 differential genes, with 80 upregulated and 34 downregulated genes. To further study the biological functions of these genes, we performed a GSEA enrichment analysis using the GSEA software. The results showed an increase in pathways related to inflammatory response, KRAS signaling, cell apoptosis, and protein secretion in NCI-H929 cells, accompanied by a decrease in pathways related to cholesterol homeostasis, adipogenesis, cell cycle, and cell proliferation (Fig. 6A and B). In RPMI-8226 cells, phenylalanine deprivation predominantly increased gene expression in the

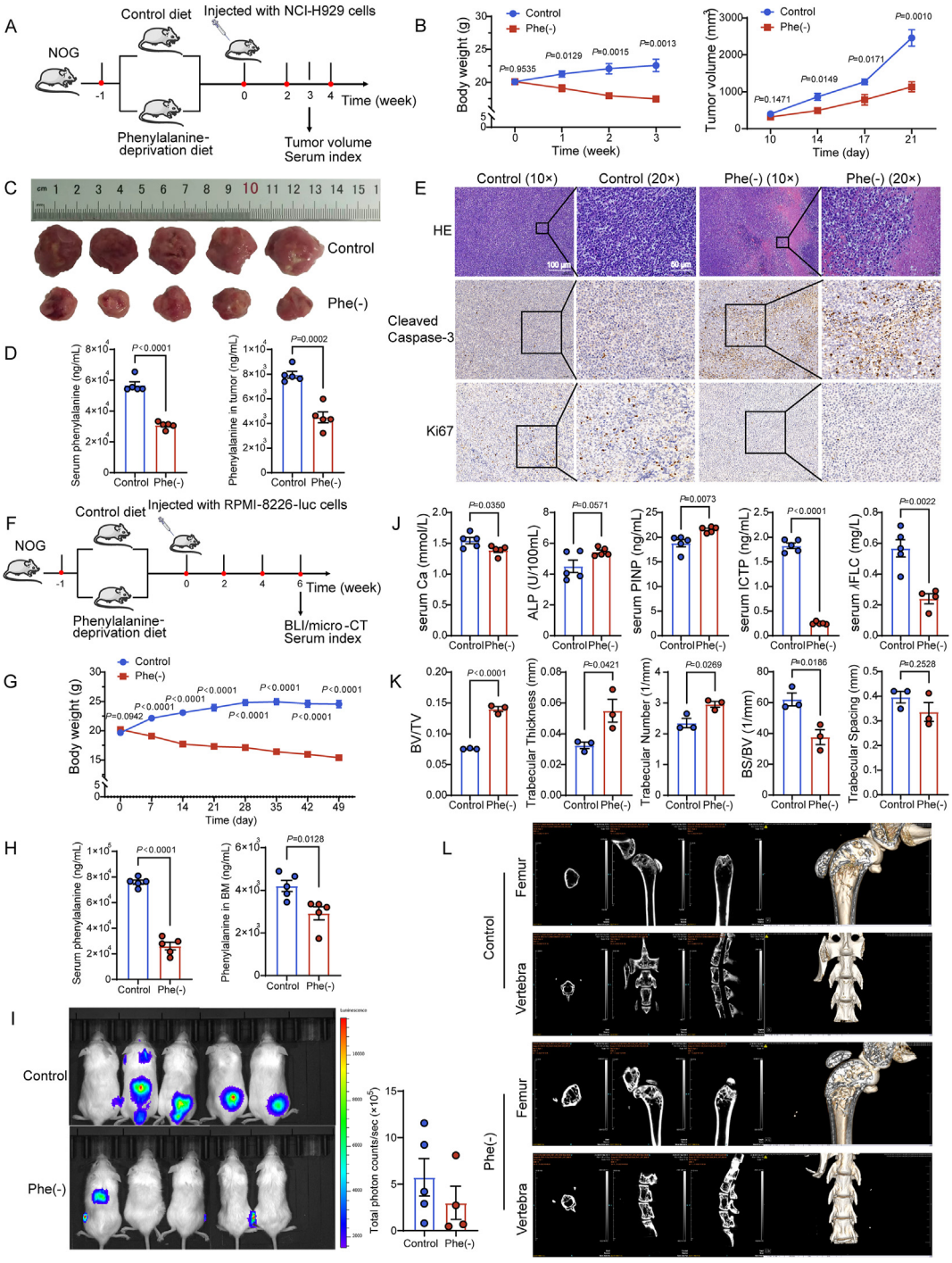

Figure 4 Phenylalanine deprivation inhibits MM *in vivo*. (A, F) Schematic of the *in vivo* experiments. (B) Alterations in mouse weight and tumor volume of the xenograft tumor model after phenylalanine deprivation. (C) Tumor nodules in NOG mice injected with NCI-H929 cells. (D) Quantitative detection of phenylalanine concentrations in serum and tumor tissues. (E) Histopathology of tumor tissues, including HE staining, cleaved caspase-3, and Ki67 immunohistochemistry for both the control and phenylalanine-deprivation groups. Scale bars: 100 and 50 μm. (G) Alterations in mouse weight. (H) Quantitative detection of phenylalanine concentrations in serum and BM tissues. (I) BLI and luminescence signal intensity of the orthotopic tumor model in the control and phenylalanine-deprivation groups. (J) Bone markers of the orthotopic tumor model after phenylalanine deprivation. (K, L) Representative 3D micro-CT images and bone parameters of the distal femur and lumbar vertebrae from each group. Data are shown as mean ± SEM; $n = 5$. Significance was analyzed with an unpaired two-sided *t*-test in (B, C, F–I).

unfolded protein response (UPR) pathway, whereas it decreased gene expression in cholesterol homeostasis, cell cycle, oxidative phosphorylation, and fatty acid metabolism pathways (Supporting Information Fig. S7A–S7C).

It has been reported that amino acid deprivation can disrupt cellular metabolic demand, destabilize endoplasmic reticulum homeostasis, and impair protein folding capabilities, thus inducing endoplasmic reticulum stress (ERS)[30]. For adaptive survival, cells

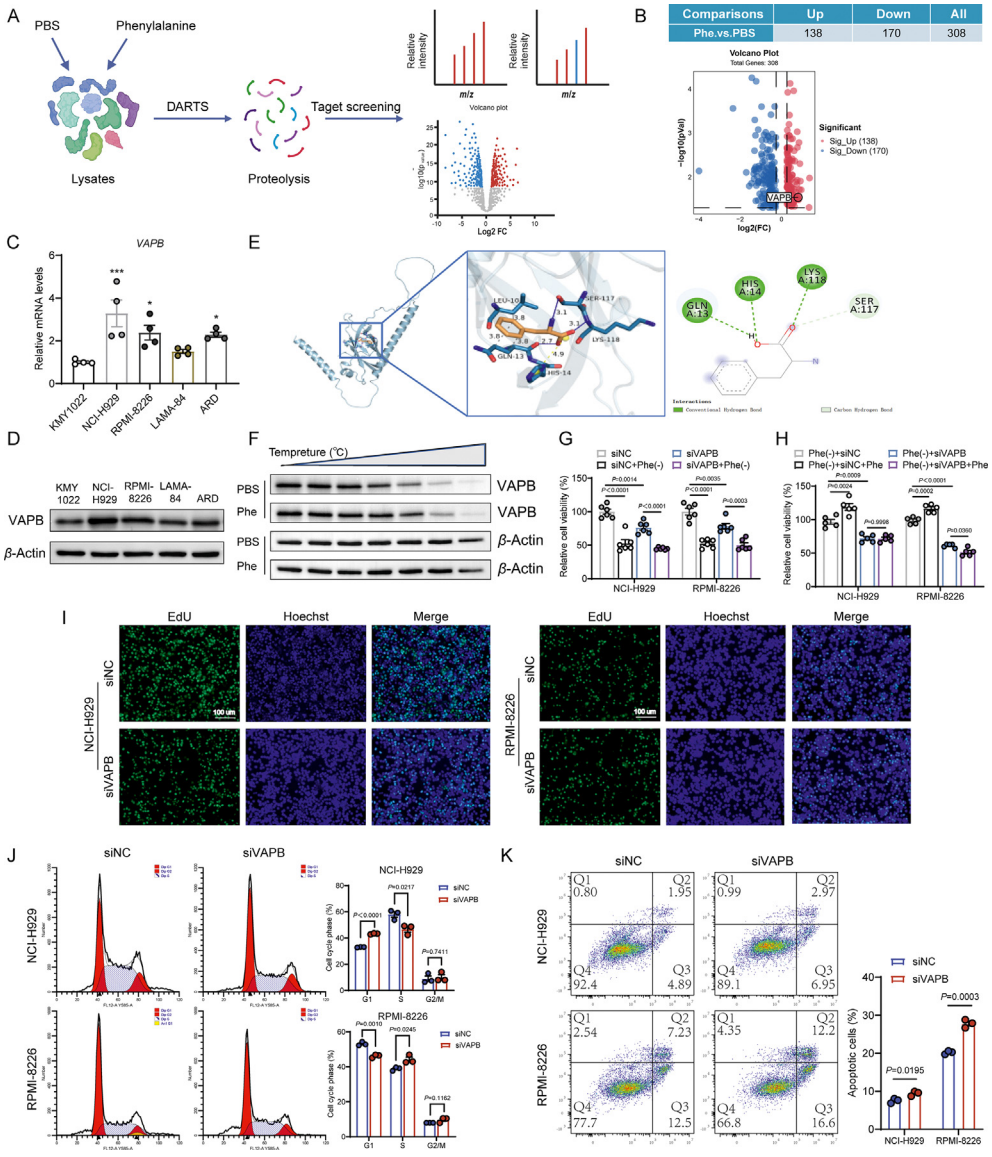

Figure 5 Direct sensor of phenylalanine in MM. (A) Schematic of the DARTS-proteomics. (Image created with BioRender.com with permission). (B) Volcano plot of differential expressed proteins. (C, D) Expression of VAPB protein in MM cells. (E) Molecular docking of phenylalanine with VAPB protein. (F) CETSA method for studying the interaction between phenylalanine and VAPB protein. (G) Interference of VAPB expression inhibits MM cell viability. (H) Phenylalanine supplementation does not restore cell viability following VAPB interference during phenylalanine deprivation. (I) Impact of VAPB expression interference on cell proliferation assessed by EDU assay. (J) Flow cytometry analysis of cell cycle following VAPB interference. (K) Flow cytometry analysis of apoptosis after VAPB interference. Data are shown as mean ± SEM; $n \geq 3$. Significance was analyzed with an unpaired two-sided *t*-test and a one-way ANOVA test. $^{*}P < 0.05$, $^{**}P < 0.01$, $^{***}P < 0.001$.

need to restore endoplasmic reticulum homeostasis. However, excessive ERS can induce cell death[30]. Our results revealed that phenylalanine deprivation can induce ERS-associated genes in the cell apoptosis pathway, as indicated by the expression of DDIT3, ATF3, and the caspase family (Fig. 6C). To investigate whether two MM cells shared the same genes, we verified the expression of DDIT3 and ATF3. We found that their expressions increased significantly and time-dependently after phenylalanine deprivation (Fig. 6D and E, Fig. S7E and S7F). Moreover, our study confirmed that the activation of ATF3 was mediated through the phosphorylation of the PERK−eIF2α pathway, an upstream signaling of the ERS pathway, whose activation is recognized as an initiating factor of ERS (Fig. 6E). However, phosphorylation of PERK−eIF2α did not activate ATF4. Instead, it specifically induces the expression of ATF3.

It has been reported that ATF3 and C/EBP homology protein (CHOP) promote cell death during the stress response[31]. Evidently, cell death under the stress of phenylalanine deprivation was observable through TEM (Fig. 6F). ATF3 regulates CHOP expression either directly or indirectly, and CHOP, in turn, can regulate ATF3 expression[32,33]. Moreover, CHOP expression can directly activate DR5 expression[34]. DR5, also known as TRAIL-R2 or KILLER, is a death receptor in the tumor necrosis factor receptor superfamily that can induce cell apoptosis when bound to its ligand

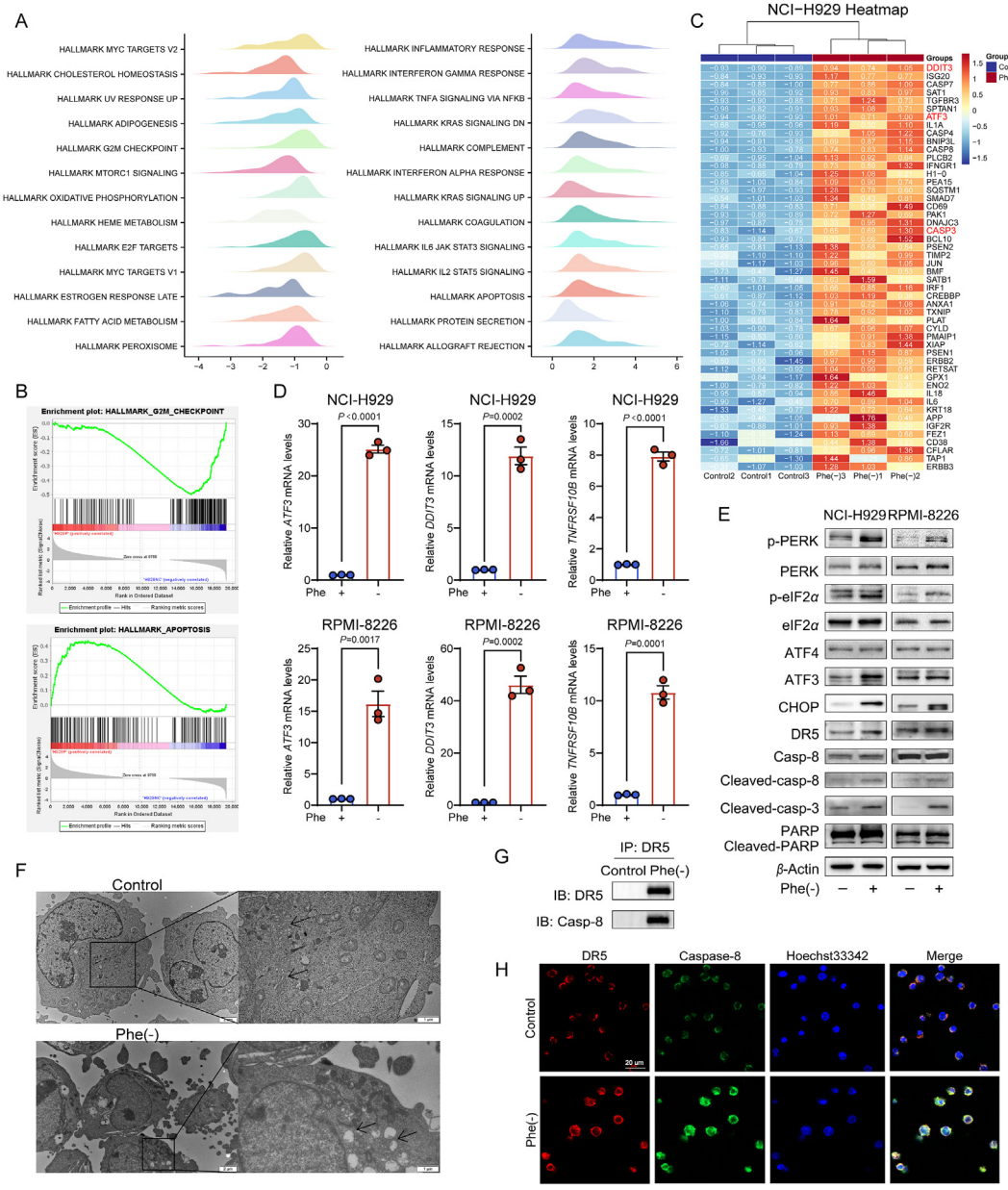

Figure 6 Mechanism of phenylalanine deprivation in inhibiting MM. (A) GSEA reveals significantly affected metabolic pathways in NCI-H929 cells after 48 h of phenylalanine deprivation using RNA-sequencing. The left chart shows the downregulated pathways, and the right chart shows the upregulated pathways. (B) GSEA analysis related to cell cycle and apoptosis pathways in NCI-H929 cells after 48 h of phenylalanine deprivation. (C) Heatmap of differential genes in the cell apoptosis pathway in NCI-H929 cells after 48 h of phenylalanine deprivation. (D) RT-qPCR shows mRNA expression of ERS related genes *ATF3*, *DDIT3*, and apoptosis related gene *TNFRSF10B* in NCI-H929 and RPMI-8226 cells after 48 h of phenylalanine deprivation. (E) Western blotting results show the protein expression of ERS and the cell apoptosis pathway in NCI-H929 and RPMI-8226 cells after 48 h of phenylalanine deprivation. (F) TEM results show nuclear condensation, cell membrane rupture, formation of apoptotic bodies, swelling, and bubble-like changes under phenylalanine deprivation. (G) Phenylalanine deprivation enhanced the recruitment of DR5 and caspase-8. NCI-H929 cells were treated under phenylalanine deprivation after 48 h. The immunoprecipitated samples were followed by Western blotting analysis to determine the expression of DR5 and caspase-8. (H) DR5 co-localized with caspase-8 on the cytomembrane of NCI-H929 cells. Immunofluorescence staining of DR5 (red) and caspase-8 (green) was treated under phenylalanine deprivation, respectively. Data are shown as mean ± SEM; $n \geq 3$. Significance was analyzed with an unpaired two-sided *t*-test and a one-way ANOVA test.

TRAIL[35,36]. Therefore, to study whether DR5 is a direct factor in phenylalanine-induced cell apoptosis, DR5 expression was confirmed. Similar to ATF3 and CHOP, DR5 expression also exhibited a time-dependent increase in response to phenylalanine deprivation (Fig. 6D and E, Fig. S7E and S7F). To elucidate the mechanism by which DR5 mediates apoptosis, we used co-localization studies to investigate the potential interaction between DR5 and caspase-8. The results confirmed that DR5

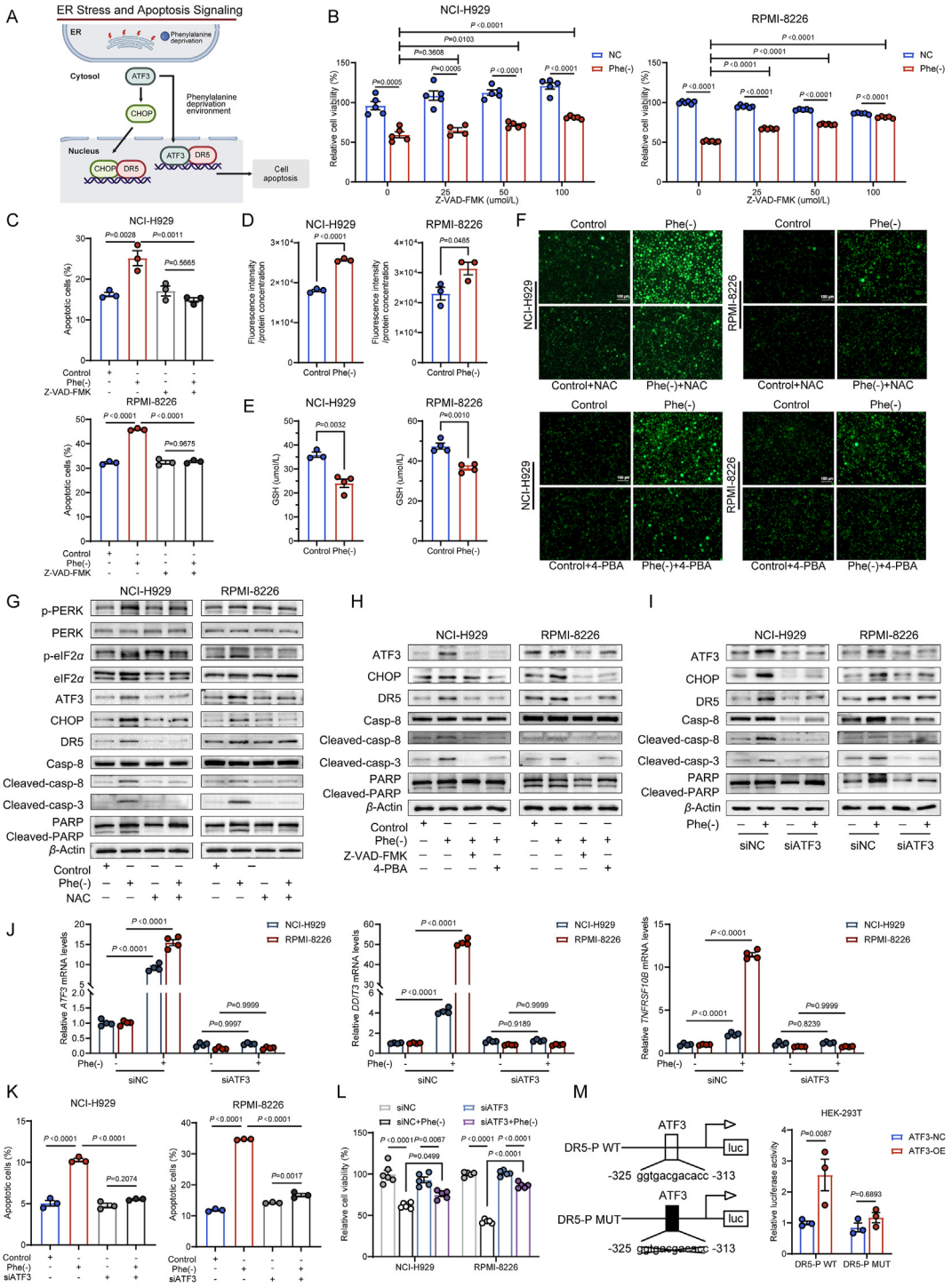

Figure 7 ATF3 is a key target in phenylalanine deprivation-induced ERS and apoptosis. (A) The relationship between ERS and the apoptosis pathway. (Image created with BioRender.com with permission). (B) Cell viability assay displays the impact of 48 h of phenylalanine deprivation combined with Z-VAD-FMK (0, 25, 50, and 100 μmol/L) in NCI-H929 and RPMI-8226 cells. (C) Flow cytometry shows the percent of apoptotic cells in NCI-H929 and RPMI-8226 cells after 48 h of phenylalanine deprivation combined with Z-VAD-FMK (50 μmol/L). (D, E) ROS and GSH levels in NCI-H929 and RPMI-8226 cells after 48 h of phenylalanine deprivation. (F) ROS levels in NCI-H929 and RPMI-8226 cells after 48 h of phenylalanine deprivation combined with NAC (5 mmol/L) or 4-PBA (1 mmol/L). (G) Western blotting results show the proteins expression of ERS and the cell apoptosis pathway in NCI-H929 and RPMI-8226 cells after 48 h of phenylalanine deprivation combined with NAC (5 mmol/L). (H) Western blotting results show the expression of ATF3, CHOP, DR5, and apoptosis-related proteins in NCI-H929 and RPMI-8226 cells after 48 h of phenylalanine deprivation combined with Z-VAD-FMK (50 μmol/L) and 4-PBA (1 mmol/L). (I) Western blotting results show the expression of ATF3, CHOP, DR5, and apoptosis-related proteins in NCI-H929 and RPMI-8226 cells after 48 h of phenylalanine deprivation with siATF3 transfection. (J) RT-qPCR shows the mRNA expression levels of *ATF3*, *DDIT3*, and *TNFRSF10B* genes in NCI-H929 and RPMI-8226

interacted with caspase-8 when phenylalanine deprivation, facilitating the formation of the death receptor complex, thereby triggering apoptosis (Fig. 6G and H). This process includes the cleavage of downstream signaling molecules, caspase-3, and PARP (Fig. 6E). Moreover, in tumor tissues from the NCI-H929 mouse model, the increased level of ERS and cell apoptosis under phenylalanine deprivation was consistent with cellular results (Fig. S7D). In conclusion, RNA sequencing revealed that phenylalanine deprivation induced severe ERS and led to apoptosis in MM through the activation of the ATF3-CHOP-DR5 pathway.

3.7. ATF3 is a crucial target in phenylalanine deprivation-induced ERS and apoptosis

We have demonstrated that the deprivation of phenylalanine can induce apoptosis in MM cells through the action of ATF3, CHOP, and DR5, as depicted in Fig. 7A. Using the pan-caspase inhibitor Z-VAD-FMK, we confirmed that the cell death was mediated by caspase-dependent pathways (Fig. 7B and C). To further investigate whether other models of cell death were involved in phenylalanine deprivation, we used inhibitors of autophagy, ferroptosis, and programmed cell death. Nevertheless, no inhibitor restored cell viability, further underscoring the role of caspase-mediated apoptosis (Supporting Information Fig. S8A−S8D). Intriguingly, we observed that the apoptosis induced by phenylalanine deprivation appeared to be dependent on ERS, as evidenced by a significant increase in ROS levels and a decrease in GSH levels (Fig. 7D and E). When ROS was eliminated, phenylalanine deprivation could not cause ROS production (Fig. 7F, Supporting Information Fig. S9A and S9B), ERS and activation of the apoptosis pathway (Fig. 7G). Additionally, treatment with 4-PBA, an ERS inhibitor, significantly improved cell viability and alleviated ERS under phenylalanine deprivation, indicating that phenylalanine deprivation activates ERS in MM cells (Fig. 7F, and Fig. S9C−S9E). Moreover, 4-PBA was found to inhibit the expression of ERS-associated ATF3 and CHOP, as well as reduce the expression of apoptotic proteins under phenylalanine deprivation (Fig. 7H and Fig. S9F).

Previous studies have reported that both ATF3 and CHOP, as transcription factors, can activate DR5 expression, leading to cell apoptosis[37−39]. To confirm this, we designed siRNAs for ATF3 and CHOP to interfere with gene expression. The results revealed that in NCI-H929 cells, silencing ATF3, but not CHOP, reversed apoptosis induced by phenylalanine deprivation. In RPMI-8226 cells, interference with ATF3 and CHOP can inhibit ERS, reverse apoptosis, and restore cell viability (Fig. 7I−L and Supporting Information Fig. S10A). Therefore, we emphasize the importance of ATF3 in phenylalanine deprivation. Moreover, interference with the DR5 gene not only prevented apoptosis but also reversed ERS-associated proteins induced by phenylalanine deprivation (Fig. S10B−S10D). To further investigate whether ATF3 can directly activate DR5 transcription, we constructed dual-luciferase reporter gene plasmids with a DR5 promoter containing ATF3 binding sites and mutated ATF3 binding sites. After co-transfection of the ATF3 overexpression plasmid and the DR5 reporter gene plasmid into HEK-293T cells, we observed a significant increase in DR5 transcription in the wild-type construct but not in the mutant construct. This indicates that ATF3 expression directly activates DR5 transcription. During phenylalanine deprivation in MM cells, ATF3 expression was stimulated. We found that the luminescence signal was enhanced after transfection with the DR5 wild-type promoter plasmid (Fig. 7M and Fig. S10E). In conclusion, ATF3, as a key target, was significantly induced during phenylalanine deprivation, and further enhancing the expression of CHOP and DR5, bridging the gap between ERS and apoptosis.

3.8. Phenylalanine deprivation enhances the efficacy of BTZ on MM

BTZ is a first-line drug for MM; however, its clinical efficacy can be influenced by drug resistance and adverse effects. Interestingly, we observed an increase in phenylalanine levels in MM cells following BTZ administration (Fig. 8A). We hypothesize that inhibiting the utilization of phenylalanine will enhance the efficacy of BTZ on MM cells. To verify our hypothesis, different concentrations of BTZ were combined with phenylalanine deprivation in MM cells. The cytotoxicity of BTZ significantly increased when combined with phenylalanine deprivation, as evidenced by CCK8 results (Fig. 8B). Since CFZ and BTZ belong to the category of proteasome inhibitors, we have also found that CFZ can be combined with phenylalanine deprivation for synergistic therapeutic effects. However, we cannot conclude that phenylalanine deprivation can be combined with DEX and THA because of the resistance of MM cells to these two drugs (Supporting Information Fig. S11A−S11D).

We then examined whether phenylalanine deprivation could enhance the efficacy of BTZ *in vivo*. NOG mice were injected intravenously with RPMI-8226-Luc cells to establish an MM model. The control and phenylalanine-deprivation groups were intraperitoneally injected with saline and BTZ (0.5 mg/kg) twice a week. Mouse weight was recorded and showed weight loss after phenylalanine deprivation (Fig. 8E). Tumor burden was assessed by bioluminescent imaging and bone turnover markers. Results showed that the combination of BTZ and phenylalanine deprivation resulted in an almost invisible luminescence intensity, indicating a significantly better synergistic anti-MM effect than using BTZ or phenylalanine deprivation alone (Fig. 8C and D). Furthermore, the serum levels of ICTP and λFLC in the group treated with BTZ and phenylalanine deprivation were significantly lower than those in the group treated with BTZ alone. Conversely, serum PINP levels were lowest in the control group and highest in the BTZ and phenylalanine-deprivation group (Fig. 8F). This finding suggests that deprivation of phenylalanine could enhance the therapeutic efficacy of BTZ in the orthotopic transplantation MM model. We also established a xenograft MM model using NCI-H929 cells, as previously described. The control group and the phenylalanine-deprivation group were intraperitoneally injected with saline and BTZ (0.5 mg/kg) twice a week. Body weight and tumor volumes were measured (Fig. 8G and H). As shown in

cells after 48 h of phenylalanine deprivation with siATF3 transfection. (K) Flow cytometry shows the percent of apoptotic cells in NCI-H929 and RPMI-8226 cells after 48 h of phenylalanine deprivation following siATF3 transfection. (L) Cell viability in NCI-H929 and RPMI-8226 cells after 48 h of phenylalanine deprivation with siATF3 transfection. (M) Dual-luciferase reporter gene experiment of ATF3 transcriptionally activating DR5 in KEK-293T cells. Data are shown as mean ± SEM; $n \geq 3$. Significance was analyzed with an unpaired two-sided *t*-test and a one-way ANOVA test.

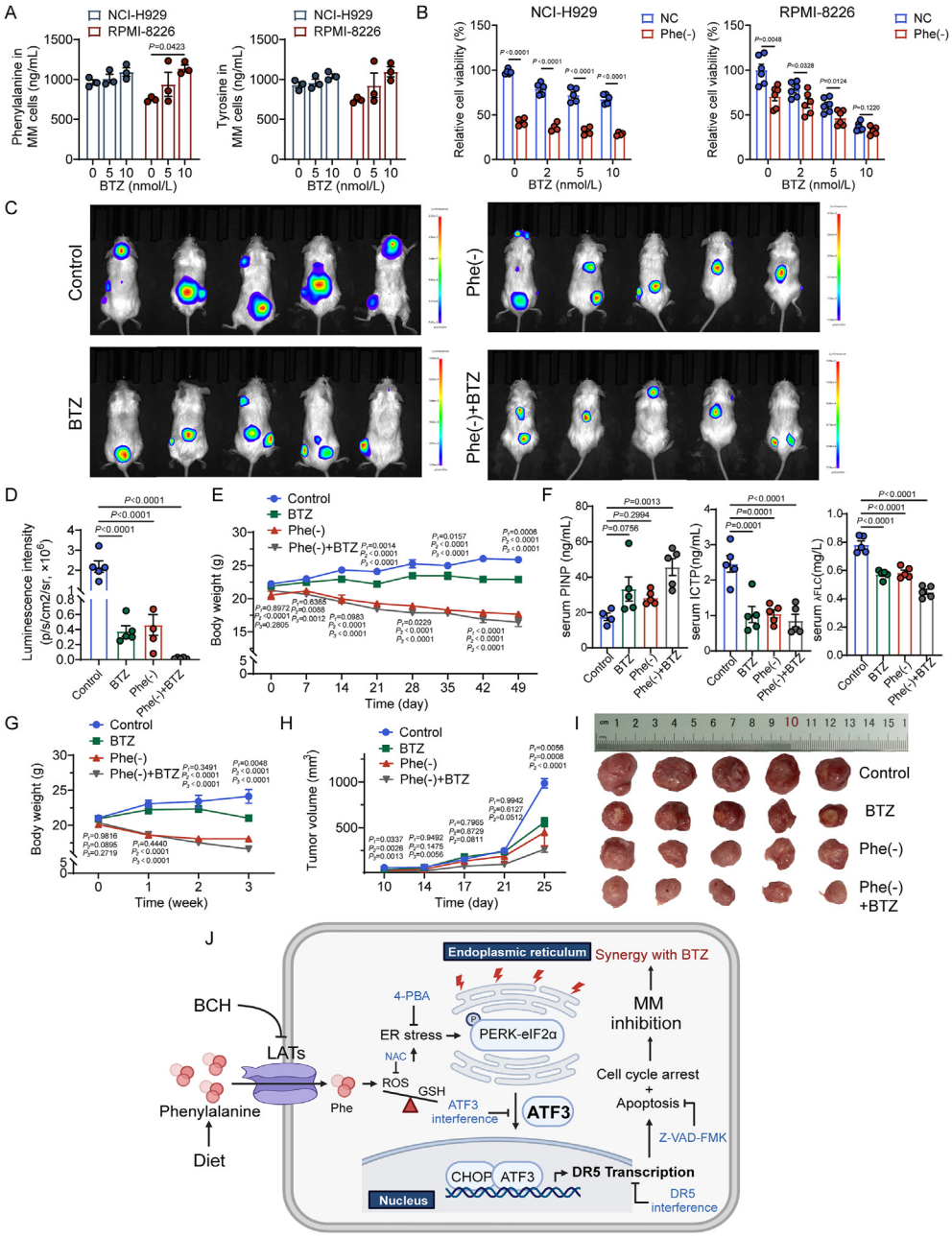

Figure 8 Phenylalanine deprivation enhances the efficacy of BTZ on MM. (A) Intracellular phenylalanine and tyrosine concentrations in MM cells treated with different doses of BTZ (0, 5, 10 nmol/L) for 48 h. (B) Cell viability of MM cells cultured in normal and Phe-free conditions, simultaneously treated with different doses of BTZ (0, 5, and 10 nmol/L) for 48 h. (C, D) BLI and luminescence signal intensity of the MM model in the groups fed with the control diet, fed with the control diet and treated with BTZ (0.5 mg/kg, twice a week), fed with the phenylalanine-deprivation diet, or fed with the phenylalanine-deprivation diet and treated with BTZ (0.5 mg/kg, twice a week). $n = 5$. (E) Alterations in mouse weight in the orthotopic transplantation MM model. (F) Quantification of bone turnover markers. (G, H) Alterations in mouse weight and tumor volume in the xenograft MM model. $n = 5$. (I) Tumor nodules in the xenograft MM model. (J) Schematic of our mechanism research. (Image created with BioRender.com with permission). Data are shown as mean ± SEM. Significance was analyzed with an unpaired two-sided *t*-test and a one-way ANOVA test.

Fig. 8I, BTZ treatment led to a significant reduction in tumor volumes, with the smallest tumor volumes observed in the combination group. These results suggest that phenylalanine deprivation could significantly enhance the therapeutic efficacy of BTZ in the xenograft MM model.

4. Discussion

Our research highlighted an explicit dependence of MM progression on phenylalanine, demonstrating its diagnostic importance in newly diagnosed patients and those receiving treatment.

We presented compelling evidence demonstrating the inhibitory effects of phenylalanine deprivation on MM cell proliferation. We examined the phenylalanine metabolic pathway *in vitro* and evaluated its impact on the TCA cycle and other organic biosynthesis pathways. Moreover, we discovered that the activation of DR5 mediates phenylalanine deprivation-induced apoptosis. Our study further demonstrated the pivotal role of ERS in phenylalanine deprivation, where the ATF3-CHOP pathway was triggered in the absence of phenylalanine, augmenting DR5 expression and exacerbating cell apoptosis (Fig. 8J). Finally, we emphasized the synergistic effect of phenylalanine deprivation and BTZ in terms of MM treatment. Our findings underscore the potential benefits of targeting phenylalanine deprivation for future MM treatment development.

Metabolomics offers insights into the fluctuations of metabolites in the biological microenvironment[40]. The BM microenvironment is a core field of metabolite exchange for MM cells. Employing metabolomic approaches permits the detection of the metabolic spectrum of the BM microenvironment, thereby enhancing our understanding of the metabolic plasticity of MM and unveiling novel intervention mechanisms. Numerous studies have investigated MM metabolomics. For instance, Du et al.[41] identified abnormal alterations in the serum metabolites of MM patients, revealing that metabolites distinguishing active MM from responding MM were enriched in the arginine and glycerophospholipid metabolic pathways. Ludwig et al.[42] examined the BM samples of patients with monoclonal gammopathy of undetermined significance (MGUS) and MM patients. They found that isoleucine, threonine, hypoxanthine, and xanthine decreased significantly. Yue et al.[43] focused on amino acid metabolites in MM serum, revealing that up-regulated metabolites such as choline and creatinine, and down-regulated metabolites such as leucine, tryptophan, and valine, possessed better diagnostic value. In addition, Ismael et al.[44] applied lipidomics to study the metabolites of newly diagnosed MM patients, shedding light on the diagnostic ability of tryptophan. Fei et al.[45] found dysregulation of plasma aspartate and threonine, as well as BM glutamate and carnitine, in MM patients. Consequently, these studies reflect potential targets for MM from different metabolite categories, which are essential biomarkers for MM diagnosis. Our research investigated differential metabolites in the plasma and BM samples from MM patients, revealing the relationship between phenylalanine in both plasma and BM. The decreased phenylalanine in PB plasma and increased phenylalanine in BM suggested that MM cells are dependent on phenylalanine. As a result, we proposed phenylalanine as a potential biomarker for MM and investigated its function in metabolic remodeling.

Cancer cells exhibit distinct metabolic requirements compared to normal cells. Limiting tumor nutrient absorption may provide novel treatment options. This therapeutic strategy is also known as nutrient deprivation therapy. For instance, glutamine is necessary for most tumor cells[46]. It provides metabolic by-products for the TCA cycle and other non-essential amino acids synthesis. Glutamine deprivation can have significant anti-tumor effects. Similarly, MM also exhibits a dependence on glutamine. Suppressing the expression of the glutamine transporter ASCT2 or the glutamine synthesis enzyme GLS1 is a novel strategy for MM treatment[47]. Arginine, a ubiquitous nutrient, is essential for the urea cycle. Arginine deprivation can result in the death of various tumor cells, and drugs targeting arginine consumption have been used in clinical trials for tumor treatments[48,49]. However, arginine consumption has a direct proliferative effect on MM. Low arginine levels were found to protect MM cells from BTZ-induced cell death and promote tumor growth *in vivo*[50]. Despite this, phenylalanine-based nutritional deprivation therapy warrants further investigation. Studies have shown that limiting phenylalanine and tyrosine significantly reduced tumor growth and metastasis in melanoma mice, induced cell cycle arrest and apoptosis, and prolonged mouse survival[51]. While reduced phenylalanine intake can result in weight loss in mice, it has no effect on the normal function of major organs. Moreover, a low-phenylalanine whey protein can alleviate osteoporosis in ovariectomized mice, demonstrating its bone-protective function[52]. Therefore, we implemented a strategy to limit phenylalanine for MM patients. This approach demonstrated significant inhibitory effects on MM progression and offered protective effects against bone marrow damage. Our results confirmed the potential of phenylalanine restriction therapy in the treatment of MM. Currently, the low-phenylalanine diet is primarily used for the treatment of phenylketonuria. We anticipate that this approach could broaden its scope of application and emerge as a promising adjuvant for the treatment of MM, although further clinical investigation is warranted.

In the future, phenylalanine will also require regular monitoring as a diagnostic marker. Elevated levels of phenylalanine can lead to the accumulation of its metabolic by-products, which can cross the blood−brain barrier and induce neurotoxic symptoms such as psychomotor retardation, disinterest in surroundings, behavioral disorders, and anxiety. Conversely, low levels of phenylalanine may result in cachexia, nutritional deficiencies, and reduced neurotransmitter synthesis, highlighting the importance of maintaining phenylalanine levels within a healthy range[53]. In our studies, we observed elevated plasma phenylalanine levels in MM patients after treatment. To address this issue, dietary interventions can be implemented to restrict phenylalanine intake and reduce plasma phenylalanine levels. Beyond traditional dietary restrictions, innovative alternatives include supplementation with neutral amino acids, bovine whey glycomacropeptides, gene therapy utilizing phenylalanine ammonia-lyase, and biological therapy with transgenic probiotics[54]. These strategies aim to lower patient phenylalanine levels while ensuring regular monitoring of blood phenylalanine to maintain it within a reasonable range. These approaches can not only normalize nutritional status and prevent the physiological outcomes associated with low phenylalanine levels but also reduce phenylalanine uptake of MM, serving as an adjunct therapy to inhibit MM progression.

Our study uncovered a connection between ERS and apoptosis triggered by phenylalanine deprivation. The reason why phenylalanine deprivation can cause ERS has been researched by our experimental evidence on the direct sensor of phenylalanine. Through proteomic analysis of phenylalanine, we found that phenylalanine can bind to the VAPB protein, which is located on the surface of the endoplasmic reticulum. A deficiency in VAPB protein or its destabilization caused by insufficient phenylalanine can disrupt endoplasmic reticulum homeostasis and cause ERS. In theory, it is also known that amino acid starvation can provoke ERS, causing cells to activate compensatory mechanisms like UPR[30]. The UPR can alleviate cellular stress by repairing incorrectly folded proteins in the cell nucleus and cytoplasm. However, irreversible ERS can cause cell death. Excessive ERS has been linked to CHOP activation, a key downstream molecule of PERK−ATF4[55]. The CHOP expression, an early-stage signal in ERS-induced apoptosis, can stimulate the transcriptional activation of various apoptosis-related proteins, such as PUMA, BIM,

BCL-2, and DR5[56]. Specially, DR5 can trigger cell apoptosis in a caspase-dependent manner. Our research found that ATF3, not ATF4, plays a role in the ERS pathway. During phenylalanine deprivation, the activation of the ATF3−CHOP−DR5 pathway induced ERS-related cell death.

It has been suggested that ATF3 is capable of exchanging with ATF4, and the activation of ATF3 is equally important during the ERS. Normal expression levels of ATF3 have been reported to be low in MM and other tumors[33,57]. However, the induction of ATF3 expression may reduce tumor growth and promote apoptosis, making ATF3 an essential mediator of apoptosis signals and a potential target for anti-cancer drugs[58,59]. Our research also clarifies the role of ATF3 in MM apoptosis induced by phenylalanine deprivation. ATF3 is significantly induced under conditions of phenylalanine nutrient deficiency, as confirmed at both the cellular and tissue levels. The expression of ATF3 further activates CHOP, which activates the transcription of DR5, initiating the extrinsic cell apoptosis signaling pathway. Our data also indicated that ATF3 could directly activate transcription of the DR5 promoter. Furthermore, as a downstream signaling molecule in the apoptosis pathway, DR5 directly contributes to ERS-induced cell death.

5. Conclusions

In conclusion, our study has demonstrated the crucial role of phenylalanine levels in MM diagnosis. Metabolites of phenylalanine and direct sensor associated with phenylalanine have been identified as essential substances for MM homeostasis. Our findings suggest that inhibiting phenylalanine metabolism could potentially serve as a therapeutic approach for MM and enhance the efficacy of BTZ treatment when used in combination. Taken together, our findings demonstrate the mechanism of phenylalanine deprivation in MM treatment. Nutrient restriction targeting phenylalanine metabolism could serve as an adjunctive therapy strategy for MM. Overall, targeting phenylalanine metabolism provides a promising avenue for further investigation of MM treatment strategies.

Acknowledgments

This study was supported by the Capital's Funds for Health Improvement and Research (CFH) (Nos. 2020-1-2031 and 2020-2-4082, China), and State Key Laboratory of Respiratory Health and Multimorbidity.

Author contributions

Longhao Cheng: Data curation, Formal analysis, Investigation, Methodology, Visualization, Writing − original draft, Software. Xiaoxue Wang: Formal analysis, Methodology, Resources, Software, Validation. Aijun Liu: Project administration, Resources, Supervision. Ying Zhu: Data curation, Resources. Hu Cheng: Validation. Jiangling Yu: Data curation, Validation. Lili Gong: Conceptualization, Project administration, Supervision, Writing − review & editing. Honglin Liu: Conceptualization, Supervision. Guolin Shen: Methodology, Project administration, Resources, Supervision. Lihong Liu: Conceptualization, Funding acquisition, Project administration, Resources, Supervision, Writing − review & editing.

Conflicts of interest

The authors declare no conflict of interest.

Appendix A. Supporting information

Supporting information to this article can be found online at https://doi.org/10.1016/j.apsb.2024.04.021.

References

1. Sung H, Ferlay J, Siegel RL, Laversanne M, Soerjomataram I, Jemal A, et al. Global cancer statistics 2020: GLOBOCAN estimates of incidence and mortality worldwide for 36 cancers in 185 countries. *CA Cancer J Clin* 2021;**71**:209−49.
2. Poh C, Keegan T, Rosenberg AS. Second primary malignancies in multiple myeloma: a review. *Blood Rev* 2021;**46**:100757.
3. Hemminki K, Försti A, Houlston R, Sud A. Epidemiology, genetics and treatment of multiple myeloma and precursor diseases. *Int J Cancer* 2021;**149**:1980−96.
4. Pavlova NN, Thompson CB. The Emerging hallmarks of cancer metabolism. *Cell Metab* 2016;**23**:27−47.
5. Li Z, Zhang H. Reprogramming of glucose, fatty acid and amino acid metabolism for cancer progression. *Cell Mol Life Sci* 2016;**73**:377−92.
6. Du D, Liu C, Qin M, Zhang X, Xi T, Yuan S, et al. Metabolic dysregulation and emerging therapeutical targets for hepatocellular carcinoma. *Acta Pharm Sin B* 2022;**12**:558−80.
7. Yoo HC, Yu YC, Sung Y, Han JM. Glutamine reliance in cell metabolism. *Exp Mol Med* 2020;**52**:1496−516.
8. Hay N. Reprogramming glucose metabolism in cancer: can it be exploited for cancer therapy?. *Nat Rev Cancer* 2016;**16**:635−49.
9. Shi J, Ju R, Gao H, Huang Y, Guo L, Zhang D. Targeting glutamine utilization to block metabolic adaptation of tumor cells under the stress of carboxyamidotriazole-induced nutrients unavailability. *Acta Pharm Sin B* 2022;**12**:759−73.
10. Tabe Y, Lorenzi PL, Konopleva M. Amino acid metabolism in hematologic malignancies and the era of targeted therapy. *Blood* 2019;**134**:1014−23.
11. Cunningham A, Erdem A, Alshamleh I, Geugien M, Pruis M, Pereira-Martins DA, et al. Dietary methionine starvation impairs acute myeloid leukemia progression. *Blood* 2022;**140**:2037−52.
12. Xia J, Zhang J, Wu X, Du W, Zhu Y, Liu X, et al. Blocking glycine utilization inhibits multiple myeloma progression by disrupting glutathione balance. *Nat Commun* 2022;**13**:4007.
13. Fung MKL, Chan GC. Drug-induced amino acid deprivation as strategy for cancer therapy. *J Hematol Oncol* 2017;**10**:144.
14. Liu X, Zhao Y, Wu X, Liu Z, Liu X. A novel strategy to fuel cancer immunotherapy: targeting glucose metabolism to remodel the tumor microenvironment. *Front Oncol* 2022;**12**:931104.
15. Jin HR, Wang J, Wang ZJ, Xi MJ, Xia BH, Deng K, et al. Lipid metabolic reprogramming in tumor microenvironment: from mechanisms to therapeutics. *J Hematol Oncol* 2023;**16**:103.
16. Xia L, Oyang L, Lin J, Tan S, Han Y, Wu N, et al. The cancer metabolic reprogramming and immune response. *Mol Cancer* 2021;**20**:28.
17. Vettore L, Westbrook RL, Tennant DA. New aspects of amino acid metabolism in cancer. *Br J Cancer* 2020;**122**:150−6.
18. Knott SRV, Wagenblast E, Khan S, Kim SY, Soto M, Wagner M, et al. Asparagine bioavailability governs metastasis in a model of breast cancer. *Nature* 2018;**554**:378−81.
19. Tajan M, Hennequart M, Cheung EC, Zani F, Hock AK, Legrave N, et al. Serine synthesis pathway inhibition cooperates with dietary serine and glycine limitation for cancer therapy. *Nat Commun* 2021;**12**:366.

20. Saha A, Zhao S, Kindall A, Wilder C, Friedman CA, Clark R, et al. Cysteine depletion sensitizes prostate cancer cells to agents that enhance DNA damage and to immune checkpoint inhibition. *J Exp Clin Cancer Res* 2023;**42**:119.
21. Fletcher M, Ramirez ME, Sierra RA, Raber P, Thevenot P, Al-Khami AA, et al. L-Arginine depletion blunts antitumor T-cell responses by inducing myeloid-derived suppressor cells. *Cancer Res* 2015;**75**:275−83.
22. Ji H, Song N, Ren J, Li W, Xu B, Li H, et al. Metabonomics reveals bisphenol A affects fatty acid and glucose metabolism through activation of LXR in the liver of male mice. *Sci Total Environ* 2020;**703**:134681.
23. Yang S, Hu T, Liu H, Lv YL, Zhang W, Li H, et al. Akebia saponin D ameliorates metabolic syndrome (MetS) *via* remodeling gut microbiota and attenuating intestinal barrier injury. *Biomed Pharmacother* 2021;**138**:111441.
24. Zimmermann M, Sauer U, Zamboni N. Quantification and mass isotopomer profiling of α-keto acids in central carbon metabolism. *Anal Chem* 2014;**86**:3232−7.
25. Tian H, Ni Z, Lam SM, Jiang W, Li F, Du J, et al. Precise metabolomics reveals a diversity of aging-associated metabolic features. *Small Methods* 2022;**6**:e2200130.
26. Chen R, Zou Y, Mao D, Sun D, Gao G, Shi J, et al. The general amino acid control pathway regulates mTOR and autophagy during serum/glutamine starvation. *J Cell Biol* 2014;**206**:173−82.
27. Mehdi SH, Nafees S, Mehdi SJ, Morris CA, Mashouri L, Yoon D. Animal models of multiple myeloma bone disease. *Front Genet* 2021;**12**:640954.
28. Pecoraro V, Roli L, Germagnoli L, Banfi G. The prognostic role of bone turnover markers in multiple myeloma patients: the impact of their assay. A systematic review and meta-analysis. *Crit Rev Oncol Hematol* 2015;**96**:54−66.
29. Hurchla MA, Garcia-Gomez A, Hornick MC, Ocio EM, Li A, Blanco JF, et al. The epoxyketone-based proteasome inhibitors carfilzomib and orally bioavailable oprozomib have anti-resorptive and bone-anabolic activity in addition to anti-myeloma effects. *Leukemia* 2013;**27**:430−40.
30. Chen X, Cubillos-Ruiz JR. Endoplasmic reticulum stress signals in the tumour and its microenvironment. *Nat Rev Cancer* 2021;**21**:71−88.
31. Tang Q, Ren L, Liu J, Li W, Zheng X, Wang J, et al. Withaferin A triggers G2/M arrest and intrinsic apoptosis in glioblastoma cells *via* ATF4−ATF3−CHOP axis. *Cell Prolif* 2020;**53**:e12706.
32. Shi Z, Diao D, Zhao Y, Luo Y, Li Y, Liu D, et al. C/EBP homologous protein deficiency enhances hematopoietic stem cell function *via* reducing ATF3/ROS-induced cell apoptosis. *Aging Cell* 2021;**20**:e13382.
33. Narita T, Ri M, Masaki A, Mori F, Ito A, Kusumoto S, et al. Lower expression of activating transcription factors 3 and 4 correlates with shorter progression-free survival in multiple myeloma patients receiving bortezomib plus dexamethasone therapy. *Blood Cancer J* 2015;**5**:e373.
34. Kim IY, Kang YJ, Yoon MJ, Kim EH, Kim SU, Kwon TK, et al. Amiodarone sensitizes human glioma cells but not astrocytes to TRAIL-induced apoptosis *via* CHOP-mediated DR5 upregulation. *Neuro Oncol* 2011;**13**:267−79.
35. Zlotorynski E. Apoptosis. DR5 unfolds ER stress. *Nat Rev Mol Cell Biol* 2014;**15**:498−9.
36. Park KM, Park JY, Pyo J, Lee SY, Kim HS. Induction of DR5-dependent apoptosis by PGA_2 through ATF4−CHOP pathway. *Molecules* 2022;**27**:3804.
37. Taketani K, Kawauchi J, Tanaka-Okamoto M, Ishizaki H, Tanaka Y, Sakai T, et al. Key role of ATF3 in p53-dependent DR5 induction upon DNA damage of human colon cancer cells. *Oncogene* 2012;**31**:2210−21.
38. Yoo KH, Kim DH, Oh S, Park MS, Kim H, Ha HH, et al. Transcriptome analysis upon potassium usnate exposure reveals ATF3-induced apoptosis in human gastric and colon cancer cells. *Phytomedicine* 2021;**91**:153655.
39. Chen P, Hu T, Liang Y, Li P, Chen X, Zhang J, et al. Neddylation inhibition activates the extrinsic apoptosis pathway through ATF4−CHOP−DR5 axis in human esophageal cancer cells. *Clin Cancer Res* 2016;**22**:4145−57.
40. Schmidt DR, Patel R, Kirsch DG, Lewis CA, Vander Heiden MG, Locasale JW. Metabolomics in cancer research and emerging applications in clinical oncology. *CA Cancer J Clin* 2021;**71**:333−58.
41. Du H, Wang L, Liu B, Wang J, Su H, Zhang T, et al. Analysis of the metabolic characteristics of serum samples in patients with multiple myeloma. *Front Pharmacol* 2018;**9**:884.
42. Ludwig C, Williams DS, Bartlett DB, Essex SJ, McNee G, Allwood JW, et al. Alterations in bone marrow metabolism are an early and consistent feature during the development of MGUS and multiple myeloma. *Blood Cancer J* 2015;**5**:e359.
43. Yue L, Zeng P, Li Y, Chai Y, Wu C, Gao B. Nontargeted and targeted metabolomics approaches reveal the key amino acid alterations involved in multiple myeloma. *PeerJ* 2022;**10**:e12918.
44. da Silva IDCG, de Castro Levatti EV, Pedroso AP, Marchioni DML, Carioca AAF, Colleoni GWB. Biochemical phenotyping of multiple myeloma patients at diagnosis reveals a disorder of mitochondrial complexes I and II and a Hartnup-like disturbance as underlying conditions, also influencing different stages of the disease. *Sci Rep* 2020;**10**:21836.
45. Fei F, Ma T, Zhou X, Zheng M, Cao B, Li J. Metabolic markers for diagnosis and risk-prediction of multiple myeloma. *Life Sci* 2021;**265**:118852.
46. Wise DR, Thompson CB. Glutamine addiction: a new therapeutic target in cancer. *Trends Biochem Sci* 2010;**35**:427−33.
47. Bolzoni M, Chiu M, Accardi F, Vescovini R, Airoldi I, Storti P, et al. Dependence on glutamine uptake and glutamine addiction characterize myeloma cells: a new attractive target. *Blood* 2016;**128**:667−79.
48. Missiaen R, Anderson NM, Kim LC, Nance B, Burrows M, Skuli N, et al. GCN2 inhibition sensitizes arginine-deprived hepatocellular carcinoma cells to senolytic treatment. *Cell Metab* 2022;**34**:1151−1167.e7.
49. Tomlinson BK, Thomson JA, Bomalaski JS, Diaz M, Akande T, Mahaffey N, et al. Phase I trial of arginine deprivation therapy with ADI-PEG 20 plus docetaxel in patients with advanced malignant solid tumors. *Clin Cancer Res* 2015;**21**:2480−6.
50. Trudu M, Oliva L, Orfanelli U, Romano A, Di Raimondo F, Sanvito F, et al. Preclinical evidence of a direct pro-survival role of arginine deprivation in multiple myeloma. *Front Oncol* 2022;**12**:968208.
51. Fu YM, Yu ZX, Ferrans VJ, Meadows GG. Tyrosine and phenylalanine restriction induces G0/G1 cell cycle arrest in murine melanoma *in vitro* and *in vivo*. *Nutr Cancer* 1997;**29**:104−13.
52. Bu T, Zhang L, Liu L, Yu S, Zheng J, Wu J, et al. Evaluation of the anti-osteoporotic effect of a low-phenylalanine whey protein hydrolysate in an ovariectomized mice model. *Food Funct* 2022;**13**:3957−67.
53. de Oliveira Filho JG, Carvalho A, Alves JDS, Egea MB. Next-generation probiotics as a therapeutic strategy for the treatment of phenylketonuria: a review. *Nutr Rev* 2022;**80**:2100−12.
54. Kumar Dalei S, Adlakha N. Food regime for phenylketonuria: presenting complications and possible solutions. *J Multidiscip Healthc* 2022;**15**:125−36.
55. Fang C, Weng T, Hu S, Yuan Z, Xiong H, Huang B, et al. IFN-γ-induced ER stress impairs autophagy and triggers apoptosis in lung cancer cells. *Oncoimmunology* 2021;**10**:1962591.
56. Kalimuthu K, Kim JH, Park YS, Luo X, Zhang L, Ku JL, et al. Glucose deprivation-induced endoplasmic reticulum stress response

plays a pivotal role in enhancement of TRAIL cytotoxicity. *J Cell Physiol* 2021;**236**:6666−77.
57. Fu D, Wang C, Yu L, Yu R. Induction of ferroptosis by ATF3 elevation alleviates cisplatin resistance in gastric cancer by restraining Nrf2/Keap1/xCT signaling. *Cell Mol Biol Lett* 2021;**26**:26.
58. Zhang G, Dai S, Chen Y, Wang H, Chen T, Shu Q, et al. Aqueous extract of *Taxus chinensis* var. *mairei* regulates the Hippo−YAP pathway and promotes apoptosis of non-small cell lung cancer *via* ATF3 *in vivo* and *in vitro*. *Biomed Pharmacother* 2021;**138**:111506.
59. Liu Y, Gao F, Jiang H, Niu L, Bi Y, Young CY, et al. Induction of DNA damage and ATF3 by retigeric acid B, a novel topoisomerase II inhibitor, promotes apoptosis in prostate cancer cells. *Cancer Lett* 2013;**337**:66−76.